THE JOURNAL OF BIOLOGICAL CHEMISTRY VOL. 285, NO. 41, pp. 31446–31461, October 8, 2010

NMR Structure and Ion Channel Activity of the p7 Protein from Hepatitis C Virus*[S]

Received for publication, March 15, 2010, and in revised form, June 18, 2010 Published, JBC Papers in Press, July 28, 2010, DOI 10.1074/jbc.M110.122895

Roland Montserret[‡1], Nathalie Saint[§1], Christophe Vanbelle[‡2], Andrés Gerardo Salvay[¶3], Jean-Pierre Simorre[¶], Christine Ebel[¶], Nicolas Sapay[‡4], Jean-Guillaume Renisio[‡5], Anja Böckmann[‡], Eike Steinmann[‖], Thomas Pietschmann[‖], Jean Dubuisson[6], Christophe Chipot[‡‡1], and François Penin[‡7]**

From the [‡]Institut de Biologie et Chimie des Protéines, UMR 5086, CNRS, Université de Lyon, IFR128 BioSciences Gerland-Lyon Sud, 69367 Lyon, France, the [§]Centre de Biochimie Structurale, CNRS-UMR 5048, INSERM-UMR 554, 34090 Montpellier, France, the [¶]Institut de Biologie Structurale, UMR 5075, Commissariat à l'Energie Atomique, CNRS, Université Joseph Fourier, 38000 Grenoble, France, the [‖]Department of Experimental Virology, Twincore-Center for Experimental and Clinical Infection Research, 30625 Hannover, Germany, [**]INSERM U1019, CNRS UMR 8204, Institut Pasteur de Lille, Université Lille-Nord de France, 59021 Lille, France, and the [‡‡]Equipe de Dynamique des Assemblages Membranaires, UMR 7565, CNRS, Université Henri Poincaré, 54506 Vandoeuvre-lès-Nancy, France

The small membrane protein p7 of hepatitis C virus forms oligomers and exhibits ion channel activity essential for virus infectivity. These viroporin features render p7 an attractive target for antiviral drug development. In this study, p7 from strain HCV-J (genotype 1b) was chemically synthesized and purified for ion channel activity measurements and structure analyses. p7 forms cation-selective ion channels in planar lipid bilayers and at the single-channel level by the patch clamp technique. Ion channel activity was shown to be inhibited by hexamethylene amiloride but not by amantadine. Circular dichroism analyses revealed that the structure of p7 is mainly α-helical, irrespective of the membrane mimetic medium (*e.g.* lysolipids, detergents, or organic solvent/water mixtures). The secondary structure elements of the monomeric form of p7 were determined by ^{1}H and ^{13}C NMR in trifluoroethanol/water mixtures. Molecular dynamics simulations in a model membrane were combined synergistically with structural data obtained from NMR experiments. This approach allowed us to determine the secondary structure elements of p7, which significantly differ from predictions, and to propose a three-dimensional model of the monomeric form of p7 associated with the phospholipid bilayer. These studies revealed the presence of a turn connecting an unexpected N-terminal α-helix to the first transmembrane helix, TM1, and a long cytosolic loop bearing the dibasic motif and connecting TM1 to TM2. These results provide the first detailed experimental structural framework for a better understanding of p7 processing, oligomerization, and ion channel gating mechanism.

Hepatitis C virus (HCV)[8] infection is a major cause of human chronic hepatitis, liver cirrhosis, and hepatocellular carcinoma (1). About 170 million individuals worldwide are chronically infected with HCV, and current therapy based on a combination of pegylated interferon and ribavirin is poorly tolerated and ineffective in 50% of patients. In this context, the ongoing search for new drugs and targets is very active, and the structural and functional characterization of the HCV viroporin p7 is essential for the molecular understanding of its role in HCV replication and for antiviral drug development.

HCV is a highly variable enveloped positive-stranded RNA virus, and patient isolates are classified into seven genotypes and numerous subtypes (2, 3) within the genus *Hepacivirus* of the family Flaviviridae (4). The HCV genome encodes a polyprotein precursor, NH_2-C-E1-E2-p7-NS2-NS3-NS4A-NS4B-NS5A-NS5B-COOH, of about 3,000 amino acids that is co- and post-translationally processed by cellular and viral proteases to yield 10 mature viral proteins. The latter include the structural proteins (C, E1, and E2) that constitute the viral particle; p7 and NS2, required for virus assembly; and NS3 to NS5B involved in HCV replication (reviewed in Ref. 5).

p7 is often incompletely cleaved from E2 (6), but it is likely to be a non-structural protein (7). p7 is found primarily in the endoplasmic reticulum as an integral membrane protein and

* This work was supported by CNRS and grants from the European Commission (LSHM-CT-2004-503359, VIRGIL Network of Excellence on Antiviral Drug Resistance) (to J. D. and F. P.) and the French National Agency for Research on AIDS and Viral Hepatitis (to F. P. and J. D.). An oral presentation (O-101) of the main part of this work was done at the 13th International Meeting on Hepatitis C and related Viruses (Cairns, Australia, August 2006).

[S] The on-line version of this article (available at http://www.jbc.org) contains supplemental Tables S1–S3 and Figs. S1–S4.

The atomic coordinates and structure factors (code 2K8J) have been deposited in the Protein Data Bank, Research Collaboratory for Structural Bioinformatics, Rutgers University, New Brunswick, NJ (http://www.rcsb.org/).

[1] These authors contributed equally to this work.

[2] Present address: CeCIL, IFR62, INSERM, Faculté de Médecine Laennec, F-69372 Lyon, France. Supported by the European Commission.

[3] Present address: Instituto de Fisica de Liquídos y Sistemas Biológicas, Universidad Nacional de La Plata, c.c. 565, B1900BTE La Plata, Argentina.

[4] Present address: CERMAV, UPR 5301, CNRS, 38041 Grenoble, France.

[5] Supported by the French National Agency for Research on AIDS and Viral Hepatitis.

[6] An International Scholar of the Howard Hughes Medical Institute.

[7] To whom correspondence should be addressed: IBCP, 7 Passage du Vercors, 69367 Lyon Cedex 07, France. Fax: 33-472-72-26-04; E-mail: f.penin@ibcp.fr.

[8] The abbreviations used are: HCV, hepatitis C virus; DM, *n*-dodecyl β-D-maltoside; DPC, *n*-dodecylphosphocholine; HMA, hexamethylene amiloride; HSQC, heteronuclear single-quantum correlation; MD, molecular dynamics; NOE, nuclear Overhauser enhancement; NOESY, NOE spectroscopy; p7(35–63), synthetic peptide representing amino acids 35–63 of p7; TFE, 2,2,2-trifluoroethanol; TOCSY, total correlation spectroscopy; TM, transmembrane; POPC, palmitoyloleyl-phosphatidylcholine; pS, picosiemens.

displays a topology in which both N and C termini point toward the endoplasmic reticulum lumen (8). However, an alternative topology wherein the C terminus is exposed to the cytoplasm may be adopted (9). p7 is not required for RNA replication *in vitro* but is essential for the late phase of assembly and the release of infectious HCV *in vitro* (7, 10) as well as productive infection *in vivo* (11). p7 probably acts in concert with other viral structural proteins (core, E1, and E2) and/or NS2, and its function may depend on interactions with other viral factors, such as core and/or NS2 (12–14).

p7 is a hydrophobic, 63-amino acid polypeptide comprising two predicted transmembrane α-helices connected by a short polar loop, including a conserved dibasic motif (7, 8, 15). Preliminary solid-state NMR analyses of recombinant p7 reconstituted in a phospholipid environment confirmed that p7 contains helical segments, which are slightly tilted relative to the membrane bilayer (16). p7 belongs to the family of viroporins, which contains small virally encoded membrane proteins, including M2 of the influenza virus and vpu of the human immunodeficiency virus HIV-1 (17). These polypeptides modify the membrane cell permeability to ions and small molecules. Isolated p7 reconstituted in artificial membranes has been reported to form oligomers and to possess cation channel activity, which is inhibited by long alkyl chain imino-sugar derivatives (18), amiloride compounds (19), and amantadine (20), albeit the latter appeared to be genotype-dependent (21, 22). Nevertheless, the relationship between the ion channel activity and the role of p7 in assembly and release of infectious HCV particles in cell culture is not known.

Electron microscopy studies revealed that p7 monomers could assemble into hexamers (20, 23) or heptamers (24) in artificial membranes. Single-particle electron microscopy recently allowed the three-dimensional structure of the hexameric p7 ion channel to be determined at 16 Å resolution, revealing a flower-shaped protein architecture with six protruding petals oriented toward the endoplasmic reticulum lumen (23). However, no detailed structure of p7 monomers has been reported hitherto, and currently proposed p7 models are based on secondary structure predictions (23–26). Electrophysiology experiments indicate that the predicted N-terminal helix lines the p7 oligomer pore (27, 28), a finding consistent with proposed p7 oligomer models.

In the present study, we report the ion channel activity of chemically synthesized p7 reconstituted in artificial membranes. Moreover, we combined NMR analyses and molecular dynamics simulations in a palmitoyloleyl-phosphatidylcholine (POPC) lipid bilayer to put forth the first detailed structure of the monomeric p7 embedded in a lipid membrane. Examination of this structure model in combination with analysis of conservation and variability of p7 amino acids among representative HCV genotypes allowed us to highlight the essential structural features of p7, which are determinants of the ion channel gating mechanism or may be associated with its role in facilitating HCV particle assembly and release from infected cells. The p7 monomer model reported here provides an experimental template for further investigations of the p7 ion channel gating mechanism and for the development of antiviral drugs.

EXPERIMENTAL PROCEDURES

Sequence Analyses—Sequence analyses were performed using tools available at the Institut de Biologie et Chimie des Protéines (IBCP) (*i.e.* the Network Protein Sequence Analysis (NPSA) Web site) (29). Provisional and confirmed genotyped HCV p7 sequences were retrieved from the European HCV Database (3). Multiple-sequence alignments were performed with ClustalW (30), using the default options.

Peptide Synthesis and Purification—The full-length p7 was synthesized chemically by solid-phase synthesis by Dr. G. Bloomberg at the Peptide Synthesis Unit of the Department of Biochemistry (University of Bristol, Bristol, UK). N-terminal and C-terminal p7 peptides 1–34 and 35–63 (denoted p7(1–34) and p7(35–63), respectively)[9] were synthesized by Clonestar Biotech s.r.o. (Brno, Czech Republic). The full-length p7, p7(1–34), and p7(35–63) peptides were purified by reversed-phase HPLC on a Vydac C8 column (300 Å, 10 μm, 10 × 250 mm) using a water/acetonitrile gradient containing 0.1% trifluoroacetic acid (31), and their molecular masses were confirmed by mass spectrometry. The purity of the full-length p7 and p7(35–63) peptides (>98%) was checked by reversed-phase HPLC, mass spectrometry, and NMR spectroscopy.

Planar Lipid Bilayer Assay—Virtually solvent-free planar lipid bilayers were formed as described (31, 32) over a 100–150-μm hole in a polytetrafluoroethylene film (10 μm thick) pretreated with a mixture of 1:40 (v/v) hexadecane/hexane and sandwiched between two half glass cells. Phosphatidylcholine from soy beans (asolectin from Sigma type IV S), dissolved in hexane (0.5%) was spread on the top of electrolyte solution (500 mM KCl, 10 mM HEPES, pH 7.4) in both compartments. Bilayer formation was achieved by lowering down and raising up the level in one or both compartments and monitoring capacity responses. Voltage was applied through an Ag/AgCl electrode in the *cis*-side, and the *trans*-side was grounded. The purified peptides dissolved in 1% DM were added in the concentration range 5×10^{-9} to 5×10^{-8} M. The peptide-containing membranes were subjected to slow ramps of potential (10 mV/s), and transmembrane currents were fed into an amplifier (BBA-01, Eastern Scientific (Rockville, MD)). Current-voltage curves were stored on a computer and analyzed with the Scope software (Bio-logic, Claix, France). For ion selectivity measurements, zero current potentials were determined by establishing a 10-fold KCl gradient (500 mM/50 mM *cis*/*trans*) across the bilayer. The ion selectivity was characterized by the ratio P_c/P_a (*i.e.* the ratio of the permeability for cations and the permeability for anions) calculated according to the Goldman-Hodgkin-Katz equation (33). All experiments were carried out at room temperature, and the bath solution of the *cis*-side compartment was stirred during the measurements.

Reconstitution of p7 into Liposomes and Patch Clamp Recordings—The purified p7 dissolved in 90% 2,2,2-trifluoroethanol (TFE) was mixed with asolectin in chloroform/metha-

[9] For consistency with standard protein chemistry nomenclature, the p7 peptide 35–63 will be referred to as p7(35–63), and residues within this peptide will be numbered from the start of the p7 protein and corresponding to HCV polyprotein residues 747–809 of strain HCV-J, genotype 1b (GenBank™ accession number D90208).

nol (1:1) (protein/lipid ratio of 1:500–1:5000 (w/w)) or 1% *n*-dodecyl β-D-maltoside (10 μM p7 in 1% DM), dried under a nitrogen flux, and lyophilized to remove any trace of solvent and water. The lyophilized sample with asolectin was directly resuspended in 2 ml of 500 mM KCl, 10 mM HEPES, pH 7.4, and sonicated in a bath sonicator until clarity. The resulting vesicle suspension was centrifuged for 20 min at 50,000 rpm at 4 °C. The lyophilized p7 sample in DM (10 μM p7 in 1% DM) was incubated with asolectin vesicles at protein/lipid ratios of 1:2000–1:5000 for 30 min at room temperature before removal of detergent by the addition of polystyrene beads (Bio-Beads SM-2 from Bio-Rad) at a concentration of 80 mg of Bio-Beads/ml of protein solution in 1% DM. After 4 h, the Bio-Beads were discarded, and the suspension was centrifuged for 20 min at 50,000 rpm at 4 °C. The pellets were suspended in 30 μl of 10 mM HEPES (pH 7.4), and aliquots were subjected to a dehydratation/rehydratation procedure to obtain giant proteoliposomes (31). For each experiment, 1–2 μl of the rehydrated suspension were placed in a 1-ml chamber containing the recording solution (500 mM KCl, 10 mM HEPES, pH 7.4). Membrane patches, obtained from unilamellar blisters from collapsing liposomes, were examined using the standard patch clamp technique (34, 35). The micropipettes used were borosilicate glass capillaries (Harvard Apparatus, Kent, UK) filled with the recording solution. The single-channel currents were visualized with the Visual Patch 500 amplifier (Bio-logic, Claix, France), and the recorded data were treated with Biotools software (Bio-logic). For the ion channel inhibition tests, we used hexamethylene amiloride (HMA) purchased from Sigma and two lots of amantadine from Sigma and Fluka.

Analytical Centrifugation—The samples were prepared from co-lyophilized p7 and $C_{12}E_8$ dissolved in a mixture of ~51% D_2O, 49% H_2O of density 1.05655 g/ml (*i.e.* the density of the detergent (36)) and viscosity 1.127 millipascal. The experiments were performed using a Beckman XL-I analytical ultracentrifuge and an AN-60 TI rotor (Beckman Coulter) in a 12-mm optical path length cell equipped with sapphire windows. Further details are provided in the legends of supplemental Fig. S2 and Table S2.

Circular Dichroism—Circular dichroism (CD) spectra were recorded on a Jobin Yvon CD6 spectrometer calibrated with (1*S*)-(+)-10-camphorsulfonic acid. The measurements were carried out at room temperature in a 0.1-cm path length quartz cuvette, with peptide concentrations ranging from 30 to 60 μM. The spectra were recorded in the 190–250-nm wavelength range with a 0.2-nm increment and a 2-s integration time. They were subsequently processed with the CD6 software, base line-corrected, and smoothed by using a third-order least-squares polynomial fit. The spectral units were expressed as a molar ellipticity/residue by using peptide concentrations determined from measurements of UV light absorbance of tyrosine and tryptophan at 280 nm (molar extinction coefficients of 1,536 and 5,600 $M^{-1}\cdot cm^{-1}$, respectively). The secondary structure content was estimated with various deconvolution methods, employing the DICHROWEB server (37).

NMR Spectroscopy—The purified p7 and p7(35–63) peptides were dissolved either in 100 mM dodecylphosphocholine (DPC)-d_{38} (>98%) or SDS-d_{25} (>98%) or in mixtures of 50–90% TFE-d_2 (>99%) in H_2O (v/v) at a final concentration of about 1.3 mM. 2,2-dimethyl-2-silapentane-5-sulfonate was added to the NMR samples as an internal ^1H chemical shift reference. The spectra were acquired at temperatures of 20 and 25 °C. Multidimensional NMR experiments were performed on a Varian Unity-*plus* 500-MHz and a Varian *Inova* 800-MHz spectrometer equipped with triple-resonance 5-mm probes with a self-shielded *z*-gradient coil. NOESY (mixing times between 100 and 250 ms), clean TOCSY (isotropic mixing time of 80 ms), and ^1H-^{13}C HSQC experiments were performed with conventional optimized pulse sequences, as was detailed previously (see Refs. 38–40 and references therein). The Varian VNMR software was used to process all data, and Sparky was used for spectral analysis (T. D. Goddard and D. G. Kneller, University of California San Francisco). The resonances of protons were ascribed by the conventional assignment method (41). In short, intraresidue backbone resonances and aliphatic side chains were identified from two-dimensional DQF-COSY and TOCSY spectra, with the help of ^1H-^{13}C HSQC and HSQC-TOCSY spectra in natural ^{13}C abundance at 20 and 25 °C to resolve the overlap of resonances (42). Sequential assignments were determined by correlation of intraresidue assignments with interresidue cross-peaks observed in two-dimensional NOESY. NMR-derived ^1H α and $^{13}C\alpha$ chemical shifts are reported relative to the random coil chemical shifts in TFE (43, 44).

NMR-derived Distance Constraints and Structure Calculation—NOE intensities used as distances input for structure calculations were obtained from the NOESY spectrum recorded with a 150-ms mixing time. NOEs were partitioned into three categories of intensities, which were converted into distances ranging from a common lower limit of 1.8 Å to upper limits of 2.8, 3.9, and 5.0 Å, respectively. The cross-peak intensity of the Hδ-Hε protons of Tyr^{45} was used as the distance reference (2.45 Å). Protons without stereospecific assignments were treated as pseudoatoms, and the correction factors were added to the upper distance constraints (41). Neither additional dihedral angle nor hydrogen bond restraints were introduced. The three-dimensional structures were generated from NOE distances by means of a dynamic simulated annealing protocol, using the XPLOR-NIH 2.0.7 program (45) and standard force field and default parameter sets. Sets of 50 structures were initially calculated to sample widely the conformational space, and the structures of low energy with no distance restraint violations (>0.5 Å) were retained. The selected structures were compared by pairwise root mean square deviation over the backbone atom coordinates (N, Cα, and C′). Statistical analyses, superimposition of structures, and structural analyses were performed with MOLMOL version 2.6 (46), AQUA version 3.2, and PROCHECK-NMR version 3.5.4 (47).

Molecular Modeling of the Monomeric HCV p7 Protein—On the basis of the structural information acquired from both CD experiments in membrane mimetics and NMR structures in TFE/water solutions, a model of the complete monomeric protein was built. Because the latter experiments only supply fragments of the complete structure of p7 (see "Results"), a number of assumptions should be made when the segments of known structure are combined with those of undefined structure. The

p7 topology with both N and C termini pointing toward the endoplasmic reticulum lumen (8) indicates that the TM1 and TM2 α-helices probably form a hairpin motif that spans the entire hydrophobic core of the membrane. The construction of this motif, which implies the pairing of TM1 and TM2, was achieved by means of protein-protein molecular docking. Use was made of the GRAMM program (48) to explore α-helix association through rigid body translation and rotation of the individual helical units. An optimized scoring function was employed, the target of which was membrane proteins. Exploration was restrained to the formation of anti-parallel α-helix bundles. Among the solutions proposed by GRAMM, only those corresponding to strictly anti-parallel helical segments facing each other were retained. Selection was further narrowed down by examination of the interhelical contacts and elimination of unphysical spatial arrangements. The two TM α-helices were subsequently bridged into a hairpin by means of a short, four-residue loop domain, by using the VMD program (49). The N-terminal α-helix was then pasted to the TM1 segment, before attachment of the unstructured C-terminal fragment at the tail end of the TM2 α-helix, thus completing the model of the protein. Backbone dihedral angles were checked against rotamer libraries and corrected whenever necessary. A rapid energy minimization was then performed, with the NAMD molecular dynamics program (50) with the CHARMM27 macromolecular force field (51) to remove spurious intramolecular contacts.

Molecular Dynamics Simulation—To appraise the relevance of the p7 protein model and shed new light on the subtle balance between protein-protein and protein-lipid interactions, the monomeric HCV p7 protein was finally immersed in a membrane environment. The latter consisted of a fully hydrated POPC lipid bilayer, which had been preliminarily thermalized. All simulations were performed in the isobaric-isothermal ensemble. The pressure and the temperature were maintained at 1 bar and 300 K, respectively, employing the Langevin piston algorithm (52) and softly damped Langevin dynamics. The particle mesh Ewald method (53) was utilized to compute electrostatic interactions. The *r*-RESPA multiple time-step integrator (54) was used with a time step of 2 fs for short range and 4 fs for long range forces. Covalent bonds involving a hydrogen atom were constrained to their equilibrium length. A 40-ns trajectory was generated, over which the last 20 ns were considered for the analysis of the molecular assembly.

RESULTS

Production of p7—The full-length 63-amino acid p7 polypeptide from strain HCV-J of genotype 1b (accession number D90208; see Fig. 6*A*) was obtained by chemical synthesis. To avoid any unexpected disulfide bond formation during CD and NMR experiments, cysteine 27 was replaced by an alanine (see sequence in Fig. 6*A*, mutC27A HCV-J). The choice of Ala instead of Ser for the mutation of Cys^{27} was motivated by the investigation of Griffin *et al.* (15), who reported that a C27A mutation results in only a slight reduction in p7 activity in a cell-based hemadsorption surrogate assay. In addition, no p7 sequence variant incorporating a Ser at position 27 was ever reported among the 1325 sequences available to date in the HCV sequence databases (3). It should be noted, however, that Thr is observed in some variants, albeit only those of genotype 2b. In contrast, one p7 sequence featuring an alanine at position 27 was reported (accession number AY232730), and 1.7 and 1.6% of the reported sequences include helix-stabilizing residues Val and Ile, respectively. Therefore, we expected that alanine at position 27 would not disturb the predicted p7 helical folding in the corresponding region as well as the functionality of p7. The chemical synthesis of full-length p7 as well as syntheses of p7(1–34) and p7(35–63) were successful, yielding a crude product containing predominantly the expected peptide, as checked by electrospray mass spectroscopy. Further purification by reversed-phase HPLC allowed us to prepare highly purified full-length p7 (>98%), albeit with a rather low yield (about 16%) (31). The p7(35–63) peptide could also be highly purified by reversed-phase HPLC. In contrast, the p7(1–34) peptide appeared to be very difficult to purify and was only obtained in low amounts with about 85% purity.

p7 Ion Channel Properties—In order to check and investigate ion channel forming activity of the purified full-length p7 C27A, the latter was first incorporated into planar lipid bilayers in the presence of symmetrical salt solutions. Current recordings in response to a triangular voltage ramp applied to an asolectin bilayer containing p7 are shown in Fig. 1*A*. These experiments performed in 500 mM KCl solution revealed a non-linear current-voltage curve, indicating that conductance characteristics of p7 are a function of the membrane potential. Moreover, p7 showed a clearly asymmetric behavior in this current-voltage diagram (*i.e.* it exhibits higher current values at negative voltages than at the corresponding positive voltages when added to one side of the planar lipid bilayer). It can also be observed from the current-voltage (I/V) curve that p7 channels remained open for a longer period at positive voltages than at the corresponding negative ones, as indicated by a broader hysteresis of the curve in the positive quadrant. It is noteworthy that this rectification is minimal when a larger amount of p7 protein is incorporated into the planar lipid bilayer (see I/V curves in Fig. 1*B*).

Measurements of ion selectivity were performed in a multichannel experiment by measuring the membrane potential developed by a salt gradient across the p7 channels at zero current conditions (see supplemental Table S1). The potential obtained for a 10-fold KCl gradient (500 mM KCl in *cis*-side, 50 mM KCl in *trans*-side) was negative (*i.e.* the potential becomes negative on the side with the higher electrolyte solution, denoting that p7 ion channel is cation-selective). The mean value of this potential corrected from the liquid junction potential was −41.0 ± 2.2 mV (average from four independent experiments) and resulted in a corresponding permeability ratio $P_{K^+}/P_{Cl^-} \approx 11$ calculated by the Godlman-Hodgkin-Katz equation.

The channel activity of p7 was confirmed by examining isolated membrane patches from proteoliposomes containing p7 by the patch clamp technique. At a 1:5000 protein/lipid ratio, channel activity was observed in about 20–30% of the liposome patches. As shown in Fig. 2*A*, this ion channel activity was found to be asymmetric according to the voltage polarity (*i.e.* the maximum value of current is larger at negative voltage). This asymmetric behavior, highly reproducible, as observed for

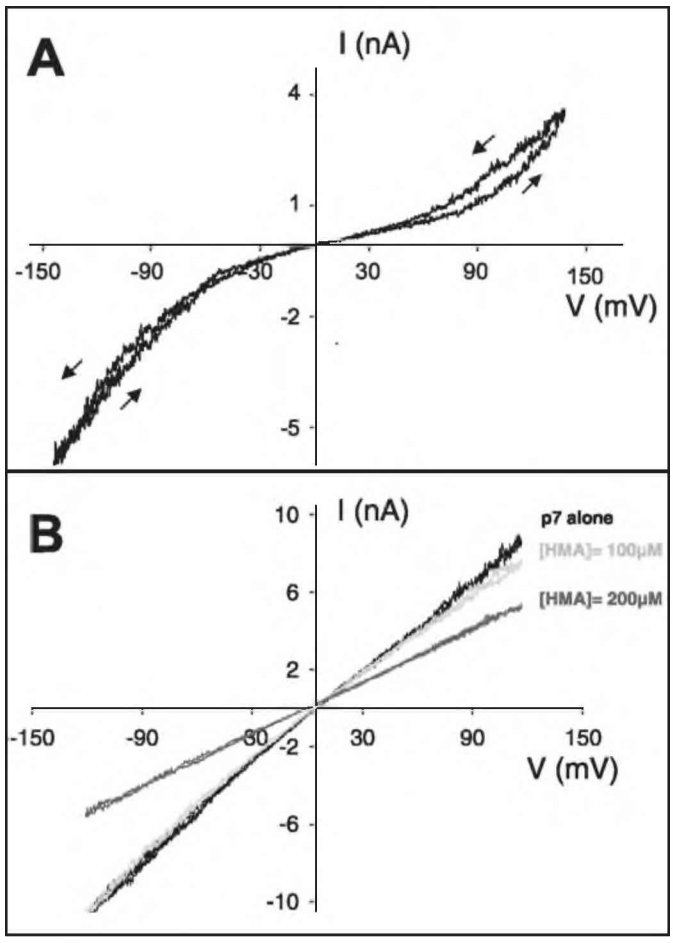

FIGURE 1. **Current-voltage relationship of p7 as measured by the response to a slow potential ramp of ±150 mV to an asolectin bilayer.** p7 protein (5 nmol of 10 μM p7 stock solution in 1% DM) was added to the *cis* side of the membrane bathed in 500 mM KCl, 10 mM HEPES, pH 7.4. The *arrows* indicate the direction of the applied voltage ramp. *A*, I/V curve of p7. *B*, I/V curve of p7 in the presence of HMA. Note that the I/V curve in *A* shows a low rectification of the current and an asymmetric current (more current at negative potential). In the I/V curve in *B*, the current is still asymmetric (always a larger current at negative potential), but the rectification is minimal. This is due to the fact that the amount of p7 protein incorporated into the bilayer is more important that in *A*.

measurements in planar lipid bilayers, indicated that p7 molecules would insert in a preferred orientation into planar lipid bilayers as well as into liposomes. Current recordings obtained at positive voltages from liposome containing p7 showed better defined current fluctuations than those recorded at negative potentials. The major channel conductance values observed at +60 and +140 mV were 22 ± 6 and 41 ± 8 pS, respectively, in 500 mM KCl, 10 mM HEPES, pH 7.4. At negative voltages, the conductance levels became less resolved, but an increase in single-channel conductance values by a factor of ~2–3.5 over the channels recorded at corresponding positive potentials could be detected. With liposomes containing a larger amount of p7 (protein/lipid ratio, 1:500–1:2000), 50–60% of the patches were found to present a functional p7 protein. The current recordings obtained in these conditions resulted, however, in observation of multiple conductance level channels (marked *0*, *1*, *2*, and *3* in Fig. 2*B*). The conductance values 35, 57, 120, and 184 pS observed in these conditions (500 mM KCl, 10 mM HEPES, pH 7.4) could represent the insertion of simultaneous channels, although we cannot exclude the possibility that level 3 is a second conductance state of the channel with one more monomer in the conducting channel.

The p7 Ion Channel Activity Is Blocked by HMA but Not by Amantadine—It was previously reported that the p7 channel can be blocked by amantadine (20) and HMA (19). We indeed observed that the ion channel activity of our p7 peptide was inhibited by HMA in a concentration-dependent fashion (Fig. 1*B*). The amplitude of the I/V curve of p7 without drug was reduced by about 40–50% in the presence of 200 μM HMA. In a previous study, Premkumar *et al.* (19) reported an inhibition of the current with 100 μM HMA through single channels of p7 of genotype 1a (strain H77). However, in accordance with our data, these authors mentioned that HMA did not completely block the channel activity with larger currents. In contrast, no inhibition by amantadine could be measured, regardless of the concentration used from 100 μM to 1 mM. Oddly enough, we observed that amantadine had a tendency to favor ion fluxes passing through p7 channels because the amplitudes of the I/V curves were increased after the addition of this drug (data not shown).

To determine which part of p7 was responsible for its ion channel activity, peptides p7(1–34) and p7(35–63), corresponding to the N- and C-terminal half of p7, respectively, were synthesized. We found that the p7(1–34) peptide solubilized in 1% DM and reconstituted in planar lipid bilayers exhibited some ion channel activity. This segment displayed a heterogeneous channel activity with conductance values ranging from 25 to 240 pS in 500 mM KCl, with a predominant well defined conductance state of about 60 pS (see supplemental Fig. S1). The limited purity of the p7(1–34) peptide, which appeared to be difficult to synthesize and to purify did not allow us to demonstrate unambiguously that this peptide alone is responsible for the ion channel formation that we observed. This finding is, nonetheless, in agreement with that reported by Haqshenas *et al.* (27), who found that a peptide comprising the N-terminal 38 residues of p7 could form ion channels. The p7(35–63) segment was found to be totally insoluble in the conditions used above and could not be reconstituted in artificial lipid bilayers. This pronounced tendency toward aggregation, together with the strong overall hydrophobicity of the amino acid sequence, does not support the formation of ion channel via the C-terminal half of p7.

Analytical Centrifugation of p7 in Detergent $C_{12}E_8$—To characterize the homogeneity and oligomerization state of p7 in detergent, p7 peptide (0.4 and 0.07 mg/ml) dissolved in $C_{12}E_8$ (2 or 0.33 mg/ml) was studied by analytical ultracentrifugation in a mixture of 51% D_2O and 49% H_2O to match the density of this detergent (36). The sedimentation velocity revealed the presence of a main species together with some larger molecular weight species (see supplemental Fig. S2). Decreasing the detergent concentration increased the relative amount of larger species. The ratio of the fringe shift number obtained by interference optics and absorbance at 280 nm allowed an estimate of 12–16 molecules of $C_{12}E_8$ per p7 molecule (1–1.3 g/g). Assuming an oligomeric state for p7 (see below), this value is consistent with that reported for intrinsic membrane proteins (55). The range of the mean experimental sedimentation coefficients

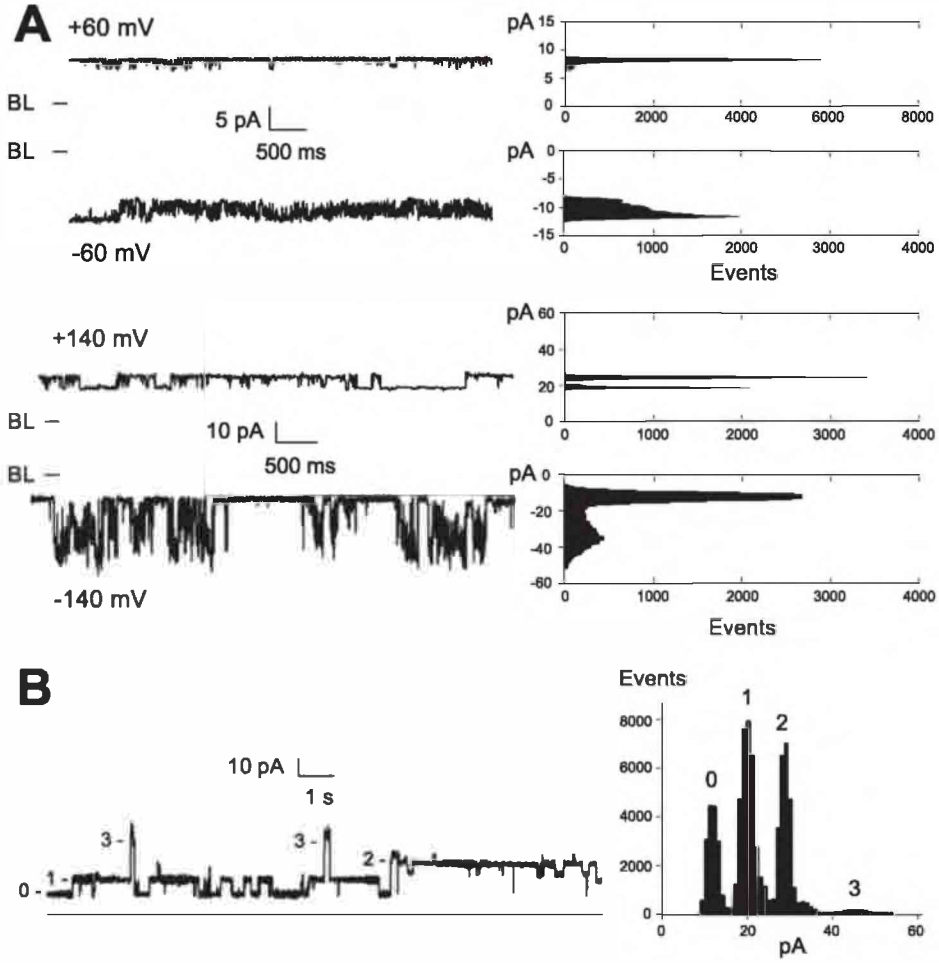

FIGURE 2. **Single-channel recordings of p7 reconstituted into asolectin liposomes and examined by the patch clamp technique in 500 mM KCl, 10 mM HEPES, pH 7.4.** *A*, channel activity is shown at two positive pipette holding potentials and at their negative corresponding potentials. The base line (*BL*) is shown as a *horizontal line*. The protein/lipid ratio is 1:5,000. An associated amplitude histogram is displayed to the *right* of each recording. *B*, channel activity is shown at a pipette holding potential of +140 mV. The protein/lipid ratio is 1:2,000. The *numbers 0*, *1*, *2*, and *3* represent the major conductance levels encountered in the selected recording, as illustrated in the associated amplitude *histogram*. *Level 0* corresponds to the closed state of the channel, and *levels 1*, *2*, and *3* correspond to conductance values of 57, 120, and 184 pS, respectively. From the current-amplitude histogram, it seems that the three detected levels could represent the insertion of simultaneous channels (*level 1*, one channel; *level 2*, two channels; *level 3*, three channels).

of 1.2 and 1.5 S at 2.0 and 0.33 mg/ml $C_{12}E_8$ are consistent with globular compact assemblies of 5–6 and 6–7 solvated p7 monomers, on average. Equilibrium sedimentation experiments (see supplemental Table S2) allowed us to determine a mean association state of 6 ± 1 subunits for p7 in the presence of 2 mg/ml $C_{12}E_8$. However, here again, the association state increased when detergent concentration was decreased. In addition, the mean association increased with time, and experiments at the highest angular velocity revealed sample heterogeneity.

Put together, these data are consistent with the hexamer and heptamer of p7 reported by others (20, 23, 24) but highlight an intrinsic heterogeneity of p7 modulated by the $C_{12}E_8$ detergent concentration. They may be further indicative of a possible natural polymorphism of the p7 oligomeric state. This relative p7 oligomer heterogeneity could, nevertheless, explain the failure of crystallization assays.[10]

[10] E. Pebay-Peyroula and D. Cannella, personal communication.

Conformation Analyses of p7 by CD—As expected from its hydrophobic nature, p7 is not soluble in water, and its secondary structure was therefore examined by CD spectroscopy after solubilization in the presence of either lysophosphatidylcholine micelles (*LPC*), or various detergent micelles (*DPC* and *SDS*), or cosolvents (TFE-water mixture; *TFE 50%*) that mimic the membrane environment (Fig. 3). These membrane mimetics were selected to reflect the various conditions in a true membrane, in order to gain a more comprehensive picture of the p7 structure. The CD spectra of p7 recorded in these membrane mimetics exhibited similar shapes and were typical of α-helical folding, with two large minima around 208 and 222 nm and a maximum around 192 nm. The various CD deconvolution methods employed indicate a predominant α-helix content ranging from 59 to 68% in lysophosphatidylcholine micelles, detergents, and 50% TFE. Increasing the TFE concentration above 50% resulted in only minor changes in the amplitude of the spectrum (data not shown), showing that the maximum α-helical folding is reached in 50% TFE. The higher α-helix content observed in TFE when compared with detergents or lysolipids could be due to the monomeric state of p7 in TFE, whereas it is expected to form oligomers in detergent micelles, as shown above in $C_{12}E_8$. In addition, TFE is known to stabilize the folding of peptidic sequences exhibiting an intrinsic propensity to adopt an α-helical structure, but such folding could be different from the native one, in particular in oligomeric structures (for an overview about TFE, see Refs. 56 and 57). CD spectral analyses indicated, nevertheless, that p7 mainly adopts an α-helical structure in lipid environment and show that 50% TFE is an appropriate medium to mimic the membrane-like environment of p7. These results validate its use to probe the secondary structure of p7 by NMR.

NMR Analyses of p7 Peptide—Preliminary NMR spectra of p7 dissolved in deuterated detergents (DPC and SDS) showed broad NMR signals due to the large size of the peptide-detergent micelle and the expected oligomerization of p7 (data not shown). Such a complex could not be analyzed by proton NMR and would require at least the preparation of recombinant ^{15}N- and ^{13}C-labeled p7. In contrast, well resolved proton and natural abundance ^{13}C NMR spectra were obtained from p7 dis-

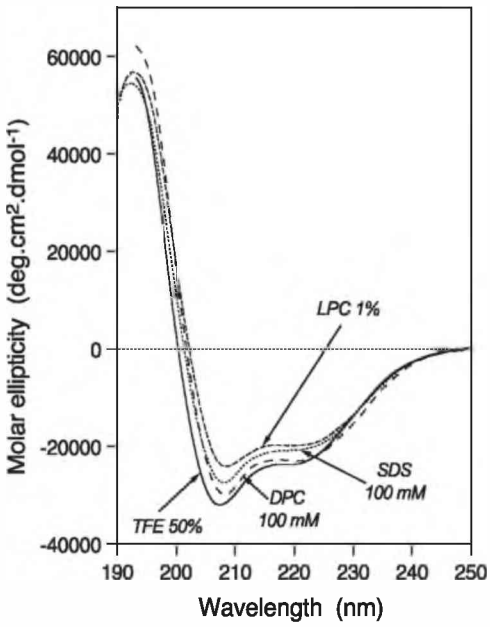

FIGURE 3. **Far-UV CD analyses of p7 in various membrane mimetic environments.** CD spectra were recorded in 5 mM sodium phosphate buffer, pH 7.5, complemented with either 1% L-α-lysophosphatidylcholine (*LPC*; *small dashed line*), 100 mM SDS (*dotted line*), 100 mM DPC (*large dashed line*), or 50% TFE (*solid line*).

solved in 50% TFE, as illustrated by the extracts reported in supplemental Fig. S3.

The limited chemical shift dispersion of p7 amide protons is typical of all α membrane proteins. Amide backbone resonances of the N-terminal half of p7 (Leu^{2}–Val^{37}) range less than 2 ppm, whereas those of the C-terminal half (Gly^{39}–Ala^{63}) range less than 0.8 ppm, overlapping the previous amide resonances. Additional assignment difficulties were due to the six consecutive leucine residues in the C-terminal half of p7 (Leu^{50}–Leu^{55}). Despite limited dispersion and overlapping of amide cross-peaks, all 58 backbone amide resonances of p7 could be assigned. The additional resolution gained with ^{13}C natural abundance HSQC and HSQC-TOCSY experiments permitted the determination of all $^{1}H\alpha$ resonances dispersed in a range of only 1 ppm. Finally, it was possible to assign all of the backbone $^{1}H\alpha$ and $^{13}C\alpha$ and most side chain ^{1}H and ^{13}C resonances. The four proline residues were identified based on their particular $^{1}H\delta$ and $^{13}C\delta$ chemical shifts and were confirmed to be in *trans* based on the ^{13}C chemical shift analysis performed with the Promega software (Shin Y and Bay A). In addition, Pro^{38} and Pro^{49} also exhibit short NOE contacts between δ-CH2 Pro and the spin system of the preceding residue. NMR analyses of the p7(35–63) peptide in the same conditions confirmed and completed the resonance assignments for the C-terminal p7 half and allowed us to gain information about the structure of this region (see below). The ^{1}H and ^{13}C chemical shift of p7 and p7(35–63) are available at the BMRB data bank under the accession numbers 6087 and 15951, respectively.

Overviews of the sequential and medium range NOE connectivities for the full-length p7 and p7(35–63) peptides are shown in Fig. 4, *A* and *B*, respectively. The N-terminal half 1–36 of p7 displays most of the characteristics of an α-helix conformation with strong $dNN(i, i+1)$ and medium $d\alpha N(i, i+1)$ sequential connectivities, weak $d\alpha N(i, i+2)$, medium $d\alpha N(i, i+3)$, medium or strong $d\alpha\beta(i, i+3)$, and weak $d\alpha N(i, i+4)$ medium range connectivities. In the remaining sequence, hatched by proline residues, similar medium range NOE contacts show the presence of an α-helical folding between Gly^{39} and Leu^{57}. The C-terminal end of the protein (Pro^{58}–Ala^{63}) is empty of medium range NOEs and remains unstructured.

The NOE-based indications of secondary structural elements are supported by the deviation of the $^{1}H\alpha$ and $^{13}C\alpha$ chemical shifts from random coil values reported in Fig. 4*C* (chemical shift index) (58). The long series of negative variation of $^{1}H\alpha$ chemical shifts ($\Delta\delta^{1}H\alpha \leq 0.1$ ppm) as well as the positive variation of $^{13}C\alpha$ chemical shifts ($\Delta\delta^{13}C\alpha \geq 0.7$ ppm) observed for residue stretches 2–14, 20–34, 38–46, and 49–55 are, indeed, typical for an α-helical conformation. The weaker negative $\Delta\delta^{1}H\alpha$ values observed for Gly^{15}, Gly^{19}, and Leu^{19} indicate the presence of some helical folding, but the absence of a clear continuous negative pattern suggests some flexibility in this region. The positive $\Delta\delta^{1}H\alpha$ and weakly positive $\Delta\delta^{13}C\alpha$ values for Leu^{36}–Val^{37} are consistent with the absence of helical folding, and the similar chemical shift pattern observed for Val^{47}-Trp^{48} is indicative of some discrepancy of the helix structure due to the presence of a proline residue at position 49. The $\Delta\delta^{1}H\alpha$ and $\Delta\delta^{13}C\alpha$ values in the C-terminal segment 56–63 are in keeping with the absence of regular structure in this region.

Put together, these results suggest that p7 protein consists of two distinct structural regions separated by an unstructured segment at the level of Gly^{34}–Pro^{38}: an ordered α-helical N-terminal region 1–34 with a flexible zone at the level of residues Gly^{15} and Gly^{18} and a C-terminal mostly helical region flanked by a flexible C terminus. Based on the NOE-derived interproton distance constraints, sets of structures were calculated with X-PLOR, and low energy structures that fully satisfied the experimental NMR data were retained (see "Experimental Procedures"). Concerning the N-terminal half of p7, two sets of structures were calculated corresponding to segments 1–18 and 18–39. Indeed, the overall structure of the 1–39 segment could not be calculated as one piece due to the lack of unambiguous distance restraints in the connecting segment 15–19. It should be noted that any attempt to fix this connecting segment 15–19 as an α-helix in structural calculations failed to yield structures satisfying the experimental NMR data, thus illuminating particular structural features for this segment. The C-terminal half of the p7 structure was calculated using the distance restraints obtained with the p7(35–63) peptide. The number and types of NOE constraints used for p7(35–63) structure calculations of p7(35–63) as well as the statistics for the final set of 30 structures are given in supplemental Table S3. The representative structure models of p7 segments are shown in Fig. 4*E*.

TFE was a very useful tool for probing the secondary structure preference of p7 and p7(35–63) and to stabilize the α-helix folding of segments exhibiting such a propensity, but a major concern is the relevance of the stabilized structure elements to their native conformation (56), in particular for p7 when oligomerized. Moreover, TFE is known to disrupt the hydrophobic

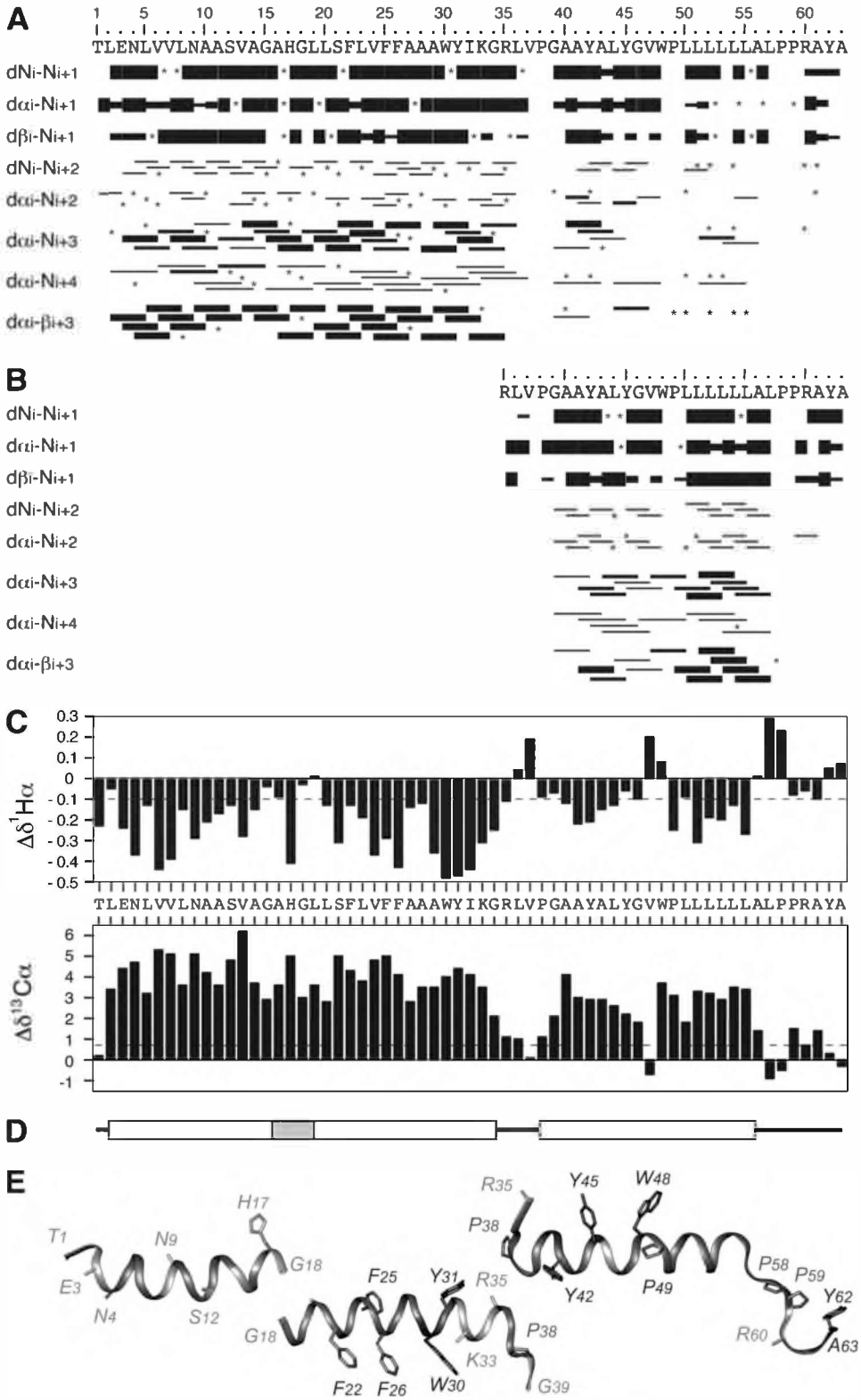

FIGURE 4. **NMR analysis and structure calculation of p7 in TFE 50%.** *A* and *B*, summary of sequential ($i, i + 1$) and medium range ($i, i + 2$ to $i + 4$) NOEs for full-length p7 and p7(35–63) peptides, respectively. Intensities of NOEs are indicated by *bar thickness*; *asterisks* indicate that the presence of a NOE is not confirmed because of resonance overlap. *C*, chemical shift differences for $^{1}H\alpha$ and $^{13}C\alpha$ at each position. These differences were calculated by subtraction of the experimental values from the random coil conformation values (43, 44). A comparison of chemical shift differences observed for segment 35–63 of full-length p7 and p7(35–63) peptides is available in supplemental Fig. S3. *D*, secondary structure elements deduced from the NMR data. The *boxes* indicate the helical elements. The *gray boxes* highlight some particular features within the helical elements (see "Results"). *E*, *ribbon representations* of NMR average calculated structures of p7 segments 1–18 (*left*), 18–39 (*medium*), and of p7(35–63) (*right*) (see "Results" for details). Cα–Cβ bonds of the polar residues (Thr, Ser, Glu, Asn, Lys, and Arg) are represented. The aromatic side chains of Phe, Tyr, and Trp as well as the cyclic side chains of Pro and His are displayed. The polar residues, including Gly, are *colored light gray*, and the other residues are *dark gray*.

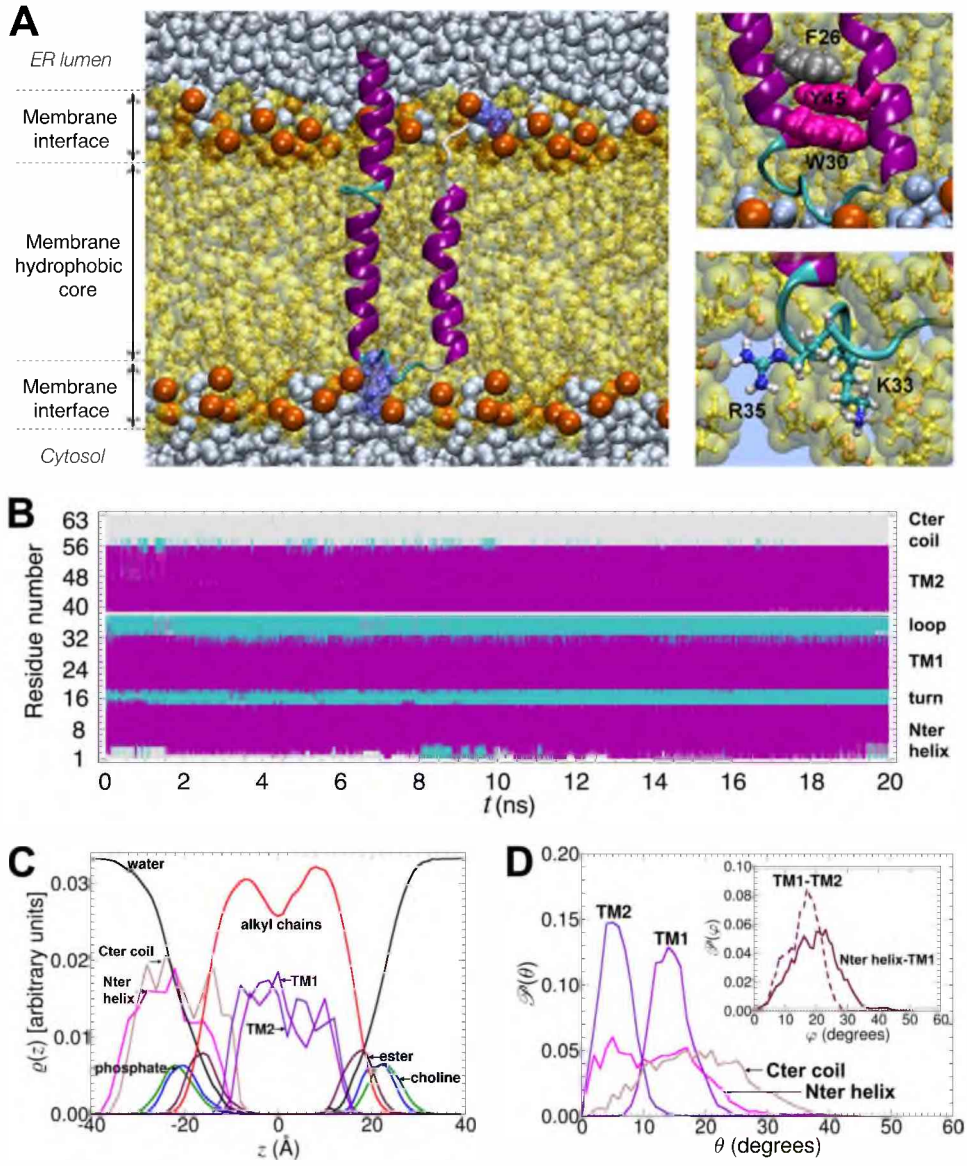

FIGURE 5. **Model of the monomeric p7 protein inserted in a fully hydrated POPC bilayer.** *A*, representative snapshot of the p7 peptide in the POPC bilayer during MD simulation. The protein backbone structure is depicted in a *ribbon and tube representation*. *Purple ribbons* denote α-helices, whereas *cyan tubes* correspond to turns. Random coils are shown as *light gray tubes*. The model lipid membrane is described by means of a *semitransparent space-filling representation* of POPC molecules, with the phosphorus atoms displayed as *glossy orange van der Waals spheres*. The positively charged Lys^{33}, Arg^{35}, and Arg^{60} residues interacting with the headgroup region of the lipid bilayer are highlighted in a *blue, semitransparent representation*. Water molecules are represented as *light blue van der Waals spheres*. *Right top inset, close up* of the TM1-TM2 interaction, whereby a double π-π stacking contributes to the overall stability of the α-helix bundle. *Right bottom inset*, interaction of the positively charged Lys^{33} and Arg^{35} residues located at the tip of the hairpin with the headgroup region of the POPC lipids. *B*, evolution of the secondary structure of p7 as a function of time. The secondary structure of the protein was determined with the STRIDE program (59). *Color coding* is as in *A*. *Nter helix*, N-terminal helix; *Cter coil*, C-terminal coil segment. *C*, density profiles for the different components of the molecular assembly depicted in *A*, determined from an average over the last 10 ns of the simulation. *D*, Jacobian corrected probability distribution of the angle φ formed by the longitudinal axis of either TM1, TM2, the N-terminal α-helix, or the C-terminal random coil and the normal to the water-membrane interface. *Inset*, probability distribution of the angle φ formed by the contiguous TM1-TM2 and N-terminal α-helix-TM1 segments. All image rendering in this figure was performed with the VMD program (49). The atomic coordinates for the representative p7 model in POPC bilayer during MD simulation is available at the IBCP website.

interactions involved in the three-dimensional structure fold and imperfectly mimic the phospholipid environment. To overcome these limitations, the reconstruction of the three-dimensional structure of the p7 monomer was done by molecular modeling and numerical simulation in a POPC membrane model by molecular dynamics.

Molecular Modeling and Molecular Dynamics Simulations of the p7 Monomer in a Fully Hydrated POPC Phospholipid Bilayer—The model of the complete p7 monomeric protein was built on the basis of the structural information acquired from CD and NMR experiments in membrane mimetics (this study) and the p7 membrane topology with both N and C termini pointing toward the endoplasmic reticulum lumen, as determined previously (8) (see "Experimental Procedures"). The relevance of this model in a membrane environment was appraised by molecular dynamics simulations of the monomeric p7 protein immersed in a fully hydrated POPC lipid bilayer (Fig. 5). Analysis of the molecular dynamics trajectory illuminates the remarkable stability of the p7 protein in its membrane environment (Fig. 5*B*). As can be seen in this panel, only marginal fluctuations in the secondary structure are witnessed in the course of the simulation (59). The core of the three helical segments is completely preserved, with merely transient fraying at the tail end of the N-terminal α-helix. The hairpin motif formed by TM1 and TM2 spans the hydrophobic core of the POPC lipid bilayer, whereas N-terminal helix and C-terminal random coil mainly lie at the membrane interface (Fig. 5, *A* and *C*). Roughly speaking, the boundaries between TM1 and the N-terminal α-helix as well as between TM2 and the C-terminal random coil emerge at the level of the ester functional groups of the lipid units. The small loop that constitutes the tip of the hairpin extends toward the headgroup region of the opposite leaflet, the positively charged residues of the former (*i.e.* Lys^{33} and Arg^{35}) interacting directly with the phosphate moieties of the latter (Fig. 5*A*). It is noteworthy that TM1 and TM2 remain anti-parallel throughout the entire run, their respective longitudinal axes being essentially collinear with the normal to the water-membrane interface. The probability distribution of the angle formed by the principal axis of each α-helix and the normal to the surface of the lipid bilayer is particularly sharp, peaking at 14° for TM1

and 5° for TM2 (Fig. 5*D*). These helix tilt angles are comparable with the ~10 and 25° tilts reported recently for recombinant p7 reconstituted in phospholipid and studied by solid state NMR (16). In contrast, the angular distribution for the N-terminal α-helix is diffuse, which is reflected in the propensity of the helical segment to tilt by up to 25° about the turn formed by residues Gly^{18} and Leu^{19}. This increased flexibility in the protein chain is further magnified at its C terminus, the random coil exhibiting a marked tendency to slant with respect to the TM orientation without any significant energetic penalty. To a large extent, stability of the monomeric p7 protein in the membrane environment can be explained in terms of a subtle balance of protein-protein and protein-lipid interactions. As has been mentioned previously, long lived interactions of the lipid units with the positively charged amino acids, either pertaining to the small loop domain or the C-terminal random coil, have been monitored. These interactions, illustrated in Fig. 5*A*, can be viewed as molecular anchors of the protein in the lipid bilayer. One possible reason for the remarkably steady antiparallel arrangement of TM1 and TM2 lies in the strength of the participating interhelical contacts. Of particular interest, as highlighted in Fig. 5*A*, the hairpin motif features a double π-π interaction formed by three stacked aromatic residues (*i.e.* Phe^{26}, Tyr^{45}, and Trp^{30}) (see supplemental Fig. S4). Displacement of the π-electron clouds with respect to each other diminishes the repulsive quadrupole-quadrupole interaction while increasing the attraction through dispersive forces. On the basis of a model of phenylalanine, a π-π interaction consisting of two optimally stacked aromatic rings has been shown to amount to about −3.4 kcal/mol (60). This π-π interaction is expected to be reinforced in the case of tryptophan, as a result of an increased dispersion contribution. In addition, cooperative effects are envisioned to tighten even further the interaction of the two TM α-helical segments. Interestingly enough, these π-π interactions were clearly absent in the original model because rigid body protein-protein docking precludes the interdigitation of the side chains to be optimized. The latter occurred at the stage of the molecular dynamics simulation, rapidly yielding an array of stacked aromatic amino acids, stable over the multinanosecond time scale.

Essential Structural Elements of p7—To highlight better the essential structural features of p7, the p7 monomer structural model was analyzed concomitantly with amino acid conservation or variability in any genotype at a given sequence position. We performed an exhaustive analysis of the p7 sequence variability based on the 1325 full-length p7 sequences of various genotypes reported to date in the public databases and documented in euHCVdb (3).

The amino acid repertoires derived from the multiple alignments revealed that, whereas the intragenotype amino acid variability is limited (61) (data not shown), the intergenotype variability is rather important at most sequence positions. This is illustrated in Fig. 6*A*, showing the sequence alignment of reference sequences representative of all major genotypes and subtypes (2). Besides the highly conserved dibasic motif bGb 33–35 in the cytosolic loop, only nine invariant amino acids emerged (labeled by an *asterisk* in the similarity pattern), thereby underlining their essential role for the structure and/or function of p7. The apparent variability at most other positions is, however, limited because the observed residues exhibit similar physicochemical properties, as indicated both by the similarity pattern (Fig. 6*A*, *colons* and *dots*) and the hydropathic pattern, where the letters *o*, *i*, and *n* denote hydrophobic, hydrophilic, and neutral residues, respectively (see the legend to Fig. 6*A* for details). Hence, despite this apparent variability, the conservation of the hydropathic character at most positions (highlighted in *gray* and *yellow* for hydrophobic and hydrophilic positions, respectively) indicates that the overall structure of p7 is conserved among the various HCV genotypes.

NMR and MD structural analyses of synthetic p7 allowed three α-helical segments to be identified, namely the N-terminal helix 2–14, the TM1 helix 19–32, and the TM2 helix 40–56 (Fig. 6*B*). The N-terminal helix is connected to the TM1 helix by a turn (15–18), and TM1 is connected to TM2 by a small loop (33–39), including the dibasic motif. The C terminus region of p7 (57–63) appears to be unstructured. TFE used here to mimic the membrane hydrophobic core is recognized to stabilize α-helical structures only in peptides or protein regions that have an inherent helical propensity (56).

The N-terminal helix observed in TFE and its stability in MD simulations in POPC clearly indicate that this helix should be folded at the level of the membrane interface and/or in p7 interactions with viral or cell factors. The physicochemical properties of this helix appear to be very well conserved among the various HCV genotypes (Fig. 6*A*), and its relatively hydrophilic nature is consistent with its location at the membrane interface (Figs. 5 and 6, *C* and *D*).

The 15–18 turn is mainly composed of small hydrophilic residues and includes residue Gly^{18}, which is fully conserved in any genotype. The quite well conserved physicochemical properties of residues 15–18 indicate that this turn is present in the p7 structure, irrespective of the genotype. Moreover, the presence of residue 17 (here His^{17}), which has been identified as one of the residues lining the pore in p7 oligomers (28), indicates that this turn is an essential structural determinant for p7 function. From a structural point of view, this turn probably constitutes a flexible link between the rigid N-terminal and TM1 helices.

Despite its apparent variability, the physicochemical properties of TM1 transmembrane helix 19–32 are rather well conserved. This helix is expected to bear the p7 pore-lining residues (see below).

The cytosolic loop 33–39 at the membrane interface contains the fully conserved dibasic motif shown to be crucial for infectivity *in vivo* as well as ion channel activity and function of the protein in virus release (7, 10, 11, 15). The conserved hydrophobic nature of segment 36–39 is consistent with its location at the hydrophilic-hydrophobic membrane interface (Figs. 5 and 6, *C* and *D*). This loop, which is longer than expected from secondary structure predictions, could confer a large flexibility between the TM1 and TM2 helices, allowing their relative reorientation, which may occur upon p7 oligomerization.

The TM2 transmembrane helix appears to be slightly bent on account of the presence of residues Pro^{49} and Gly^{46}. The full conservation of Pro^{49} in all genotypes (except for some genotype 2 subtypes and genotype 3a) on one hand and of Gly^{46} in all

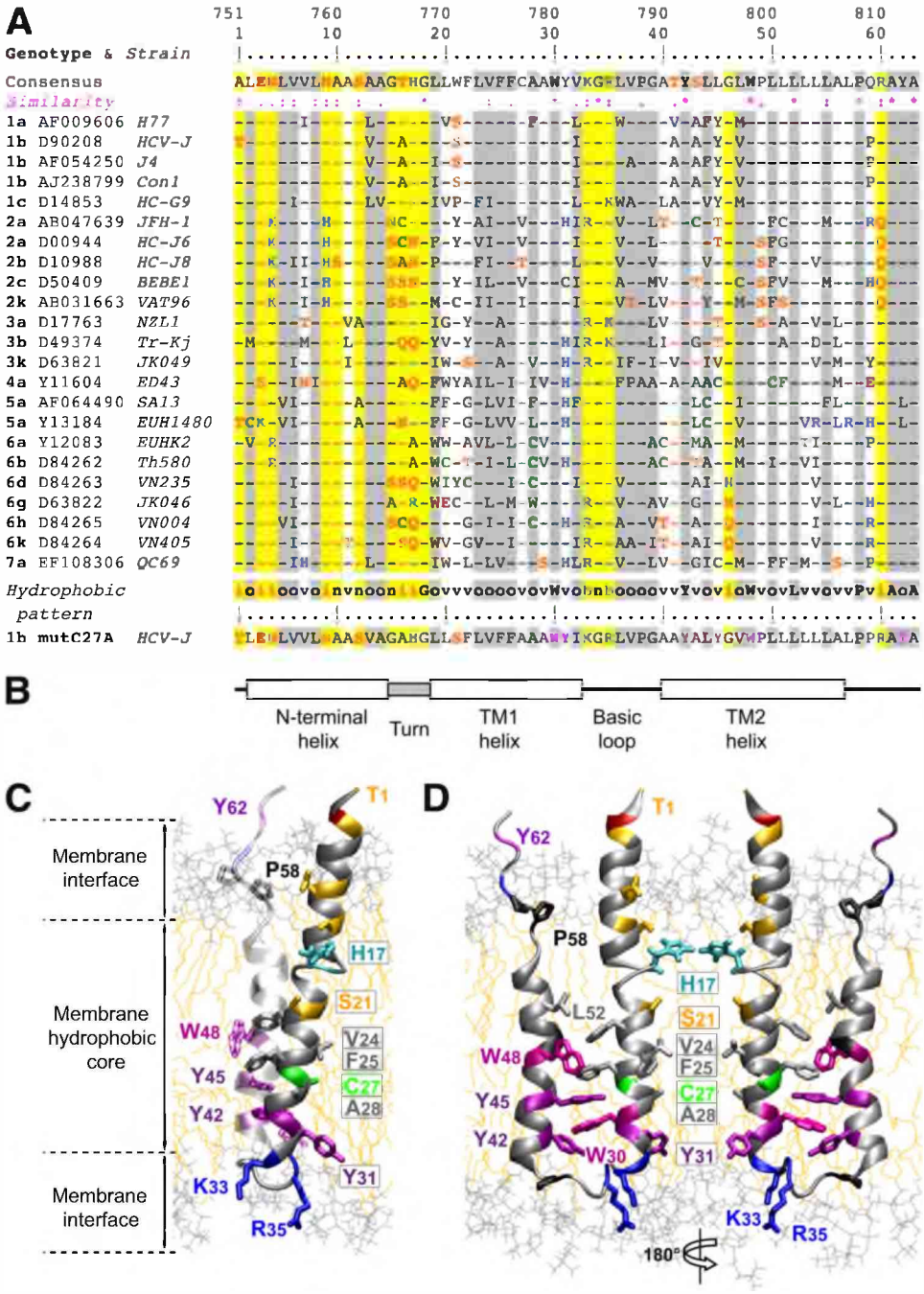

FIGURE 6. **Variability of p7 and tentative model of p7 ion channel.** *A*, multiple alignments of p7 sequences from representative HCV strains of confirmed genotypes (listed in Table 1 in Ref. 2). Genotype, accession number, and strain are indicated for each sequence. Amino acids are numbered with respect to p7, and the polyprotein of HCV strain H77 was used as a reference (77) (*top row*). The consensus sequence (*top row*) was deduced from the ClustalW multiple alignment of the indicated p7 sequences (30). To highlight the amino acids variability at each position, amino acids identical to the consensus sequence are indicated by *hyphens*. The degree of amino acid physicochemical conservation at each position can be inferred with the similarity index according to ClustalW convention (*asterisk*, invariant; *colon*, highly similar; *dot*, similar) (30) and the consensus hydropathic pattern: *o*, hydrophobic position (Phe, Ile, Trp, Tyr, Leu, Val, Met, Pro, Cys); *n*, neutral position (Gly, Ala, Thr, Ser); *i*, hydrophilic position (Lys, Gln, Asn, His, Glu, Asp, Arg); *b*, basic position; *v*, variable position (*i.e.* when both hydrophobic and hydrophilic residues are observed at a given position); strictly conserved amino acids in all genotypes are indicated with their *one-letter code*. To highlight the variable sequence positions in p7, conserved hydrophilic and hydrophobic positions are highlighted in *yellow* and *gray*, respectively. Polar and positively and negatively charged residues are *color-coded* in *orange*, *blue*, and *red*, respectively. Cysteine residues are in *green*, and all other residues are in *black*. Amino acids of the p7 sequence used in this study (1b mutC27A HCV-J, *bottom raw*) are *colored* accordingly, except for Trp and Tyr, which are *colored magenta* and *purple*, respectively, according to the p7 structure representation shown in *C* (see below). *B*, *schematic representation* of helical, turn, and loop regions deduced from the NMR structure analysis (see Fig. 4). *C*, *side view* of the p7 representative monomer structure in the POPC bilayer showing the putative helix side and residues facing the ion channel. The corresponding p7 amino acid sequence is shown in *A* (HCV-J strain). The structure backbone is represented as a *ribbon*, and only some amino acid side chains are shown, including residues likely to be involved in interhelix interactions, residues expected to be oriented toward the ion channel (*boxed labels*), basic residues of the cytosolic loop, and some residues to provide a visual reference for the orientation of p7. *Yellow*, Ser, Thr, and Asn; *green*, Cys; *cyan*, His; *blue*, Arg and Lys; *red*, Glu; *magenta*, Trp; *purple*, Tyr; *black*, Pro; *gray*, any other residues. The polar heads and hydrophobic tails of phospholipids (thin stick structures) are *light gray* and *orange*, respectively. *D*, tentative representation of p7 monomer within a putative ion channel oligomer. A 180° rotation is applied between the two structures. Images in *C* and *D* were generated from structure coordinated using the VMD program (49) and rendered with POV-Ray.

genotypes (except some genotype 6 subtypes, d, g, h, and k) on the other indicates that this bending is a specific feature of TM2. A markedly reduced channel activity was reported for recombinant P49A mutant in a liposome assay (26), which could be due to a role of TM2 bending in p7 oligomerization or other intermolecular interactions. Remarkably, the TM2 helix includes three fully conserved residues in all genotypes (*i.e.* Tyr^{42}, Trp^{48}, and Leu^{52}). The full conservation of Tyr^{42} in TM2 together with that of Trp^{30} in TM1 is consistent with their interaction through aromatic ring stacking, which contributes to the overall stability of the helix TM1-TM2 bundle in p7 monomer. In contrast, the fully conserved aromatic residue Trp^{48} does not appear to be involved in the interaction of the two TM α-helical segments. Its relatively external position in TM2 suggests that it could play an essential role in the intermolecular binding of p7 units in the oligomeric state. Leu^{52} belongs to the helical leucine-rich region 50–55 and appears to be close to Phe^{22} in TM1 of our p7 monomer model, suggesting some stabilization of the helix TM1-TM2 bundle through hydrophobic interactions. Such an interaction is, however, questionable because Phe at position 22 is poorly conserved in all genotypes. Interestingly enough, the recombinant L(50–55)A mutant was shown to retain wild-type ion channel activity in a liposome assay (26), thereby indicating that the leucine-rich region is not essential for p7 oligomer stabilization and ion channel activity. This region is in fact more likely to be involved in intermolecular interactions with other viral and/or cellular factors.

Although the C-terminal region of p7 (57–63) appears to be unstructured, it includes the three fully conserved residues Pro^{58}, Ala^{61}, and Ala^{63}. This conservation may be linked to the conformational changes required for the cleavage of the p7-NS2 junction by a signal peptidase (6, 8). It is noteworthy that high-resolution magic angle spinning NMR experiments of p7 in deuterated DPC micelles revealed some well resolved signals corresponding to residues outside the detergent micelle (data not shown). Some of them were clearly identified as alanine residues and probably correspond to Ala^{61} and Ala^{63}, as assigned by comparison with liquid state chemical shifts. This finding supports the location of segment 61–63 outside the POPC membrane in the MD p7 model (Figs. 5 and 6, *C* and *D*). Moreover, because p7 is expected to form oligomers in DPC micelles, this indicates that segment 61–63 would be accessible also in p7 oligomers. Put together, these findings suggest that the well conserved polar segment 59–63 (QPRAYA here) could also play a particular role in p7 intermolecular interactions with other viral and/or cellular factors.

Putative p7 Pore-lining Residues—The structural elements of p7 essential for its ion channel activity are not yet clearly established. However, there is a growing body of evidence pointing to the essential role of the N-terminal half of p7. Indeed, synthetic peptides corresponding to this region display ion channel-like properties (27) (this study). Moreover, point mutation analysis using recombinant p7 from strain J4 (genotype 1b) identified amino acids that are important for channel function in a liposome assay (26). Whereas mutations S21A or C27A had no effect on channel activity, H17A mutation caused a decrease in p7 channel activity. In contrast, a synthetic p7 from strain H77 (genotype 1a), including the H17A mutation, was shown to exhibit wild-type ion channel activity when reconstituted in a planar lipid bilayer (28). However, this His^{17} was shown to be involved in Cu^{2+}-mediated inhibition of channel activity of synthetic p7 from both H77 and JFH-1 strains, indicating that this His^{17} residue lines the p7 channel lumen (28). The presence of a hydrophilic serine or aromatic residue tryptophan or tyrosine in the next helix turn at position 21 (here a serine; Fig. 6*C*) suggests that this residue also faces the pore, albeit mutation S21A had no effect on channel activity (26), and proline or cysteine can also be observed at this position (Fig. 6*A*). Because the downstream helix residues facing the pore are expected to be on the same side of the TM1 helix (Fig. 6*C*), residues at positions 24 or 25 and 27 or 28 in the two next helix turns constitute pore-lining candidates (see below). Finally, because position 31 is often occupied either by a hydrophilic residue histidine or aromatic residue tyrosine bearing a polar hydroxyl group in the various HCV genotypes, residue 31 is expected to face the pore. Although determination of the high resolution structure of the oligomeric form of p7 will be required to specify the pore-lining residues, a tentative representation of a single p7 unit within a putative ion channel oligomer may be proposed as a working model (Fig. 6*D*). It should be noted that no attempt has been made here to fit this representation to the corolla-like EM hexameric structure, in which the protruding petals correspond to the subunits (23). One can suppose, however, that the p7 monomers should be tilted relative to the membrane bilayer to fit this corolla-like structure, possibly in conjunction with the kinking of the N- and C-terminal p7 structural elements.

As demonstrated in this study, alanine mutation of the candidate pore-lining residue Cys^{27} did not affect p7 channel activity *in vitro*. This is consistent with the slight reduction of activity of recombinant C27A p7 mutant from strain J4 in a cell-based hemadsorption surrogate assay (15). This Cys^{27} residue is conserved in all genotypes but genotype 2 (Fig. 6*A*). Interestingly enough, whereas hydrophobic residues valine and isoleucine instead of cysteine are observed at position 27 in subtypes a, c, and k of genotype 2, a cysteine residue is observed in the TM1 helix at position 16 (2a), 21 (2k), or 31 (2c) (*i.e.* at or close to a pore-lining residue candidate). The only subtype for which no cysteine residue was observed in p7 TM1 is 2b, but the polar residue threonine is present at position 27 in this subtype. It should be noted that in addition to residue Cys^{27}, additional cysteine residues are observed in TM1 for p7 of all subtypes of genotype 6 (except in 6k) at or close to pore-lining residue candidates. These observations indicate that a cysteine at or close to a pore-lining residue candidate is of importance for functional p7. The implication of Cys^{27} as a pore-lining residue is, however, enigmatic. Indeed, it is difficult to imagine that the probable clustering of 6–7 cysteine residues forming a ring of SH groups within the p7 oligomeric pore would be chemically neutral because disulfide bond formation could occur and would probably block the channel functioning. Alternatively, this cysteine residue might be involved in the conformational changes expected to occur upon p7 oligomer assembly and/or

in some interaction with other viral or cell factors. Finally, cysteine residues are quite commonly observed in the p7 TM2 helix of various genotypes, including 2a, 2c, 4a, 5a, 6a, 6b, and 7a. Such a high frequency of cysteine residues in p7 transmembrane segments strongly suggests the involvement of some redox mechanism in structure and/or function of p7 (*e.g.* possibly some reversible association between p7 monomers or to other viral or cell factors by disulfide-bond formation and release).

DISCUSSION

In this report, we investigated the ion channel properties and the detailed structure of a chemically synthesized p7 from HCV-J strain (genotype 1b). The ion channel activity of p7 C27A reconstituted in artificial lipid membranes is comparable with that reported by others (18, 19, 21, 28) but is shown to be resistant to amantadine inhibitor. A polymorphism of p7 oligomeric state with a mean association of 6 ± 1 subunits in $C_{12}E_8$ detergents was observed by analytical centrifugation, thereby supporting the existence of both hexameric and heptameric oligomerization of p7. Detailed structural analyses of p7 by NMR revealed significant differences with secondary structure predictions. MD simulations in phospholipids allowed us to propose a three-dimensional model of the p7 monomer, which, at least transiently, exists during HCV polyprotein biosynthesis and processing. Our studies identified structural distinctiveness elements that are conserved among HCV genotypes and probably constitute essential determinants for p7 assembly and function.

The p7 C27A polypeptide that we have synthesized for this study was found to form ion channels in lipid bilayers. Because this polypeptide was prepared chemically with a high degree of purity and without any fusion partner proteins or tags, the possibility that the channel activity might have been caused by a molecule other than p7 is unlikely. It was, therefore, concluded that Cys^{27}, conserved in p7 sequence representative of the principal HCV subtypes, was not required for a functional channel. The channel activity that we observed is not perfectly identical to those reported in previous p7 channel studies. This could be due to the fact that p7 proteins from different genotypes have been studied and/or that C27A substitution may induce some changes in the p7 structure and, consequently, on its channel properties.

The presence of a non-linearity in the p7 current-voltage curves, a characteristic also observed recently for the Vpu protein, a viroporin from HIV-1 (62), and for channel-forming peptides, such as alamethicin (63) and ceratotoxin (64), is an indicator of a voltage-dependent component to channel formation. In light of selectivity measurements, p7 channels were found to be more permeable to cations than to anions with a P_{K^+}/P_{Cl^-} ratio of about 11. Cation selectivity is a characteristic reported for other ion channels encoded by small virus proteins belonging to the viroporin family, such as M2, NB, Vpr, Vpu, and alphavirus 6K proteins (17). In a computational approach, the cation selectivity of Vpu was attributed to a ring of serine residues pointing toward the interior of the pore (65). In our p7 C27A, the serine amino acid at position 24 belongs to the list of putative residues lining the ion-conducting pore. It is, however, difficult to understand how this sole amino acid could be responsible for the strong cation selectivity that was observed. It is possible that negatively charged and hydrophilic residues (Glu^3, Asp^4, and Asn^9) from the N-terminal helix, presumably located at the membrane interface, could be involved in the cation selectivity measured for p7 as discussed below.

We have observed that p7 C27A channels as well as p7(1–34) channels could exhibit multiple conductance levels. Typically, current recordings like those displayed in Fig. 2*B* have revealed multiple states of current that could represent the insertion of simultaneous channels. However, we cannot exclude the possibility that some of these states could reflect an increase of conductance due to the association of additional transmembrane segments (*i.e.* p7 monomers) in the channel, as has been observed in α-helix bundles formed by the alamethicin and ceratotoxin peptides (63, 64). Such multiple conductance levels, which may correspond to different degrees of oligomerization of the peptide to form channels, have also been observed for the NB peptide of influenza B and Vpu (62, 66).

Inhibition of the p7 ion channel activity by HMA in our *in vitro* assay is in agreement with reported results (19). In contrast, we did not observe inhibition by amantadine, even at high concentration, whereas Griffin *et al.* (20) described the complete blocking of the p7 ion channel by 1 μM amantadine in artificial membranes. This is surprising because the sequence of p7 from strain HCV-J used in our study only features four amino acid differences with strain J4 used by Griffin *et al.* (20) (T1A, L19I, V37A, and L44F). In addition, both strains possess identical sequences in the C-terminal p7 region, where amantadine probably interacts. A p7 L(50–55)A mutant was, indeed, recently shown to exhibit resistance to amantadine (26), and the involvement of leucine residues 51–57 (with the exception of Leu^{53}) in amantadine interaction was recently confirmed by NMR and also probably includes His^{17} (16). We cannot exclude the possibility that the absence of ion channel inhibition by amantadine for our p7 peptide might be related to the substitution of Cys^{27} by alanine. Alternatively, the discrepancy in amantadine inhibition data may be due to the different p7 protein constructs that were utilized. We, indeed, used here a synthetic p7 peptide, whereas Griffin *et al.* used recombinant fusion proteins GST-p7 and GST-HIS-p7 (15, 20) or GST-FLAG-p7 and FLAG-p7 (24), which may exhibit differences in their properties. In addition, the differences between proteoliposome reconstitution and the lipid systems utilized could also have some influence because amantadine was demonstrated to bind preferentially in the interfacial region of the lipid bilayer on the basis of molecular dynamics simulations (67). This could explain why we observed in our measurements an increase of the current upon the addition of amantadine. It is possible that binding of amantadine to the membrane interface might stabilize an open conformation of the p7 channel, hence resulting in larger ion fluxes.

Molecular dynamics simulations of the monomeric p7 NMR structural model in a POPC membrane environment not only appraise the relevance of the protein model but also help to dissect the participating protein-protein interactions and shed

new light on the subtle protein-lipid interplay. These coupled structural analyses allowed three α-helical segments to be identified, namely the N-terminal helix (residues 2–14), the TM1 helix (residues 19–32), and the bent TM2 helix (residues 40–56). The N-terminal helix is connected to the TM1 helix by a turn (residues 15–18), and TM1 is connected to TM2 by a small loop (residues 33–39), including the dibasic motif. The C terminus region of p7 (residues 57–63) appears to be unstructured.

Some elements of this structural organization differ substantially from predicted secondary structures used for the molecular modeling of p7 monomer and oligomers (8, 24–26). Indeed, neither the N-terminal helix nor the turn was predicted, the cytosolic loop is longer, and the TM2 helix ends at residue 56.

The turn between the N-terminal and TM1 helices is a major finding, which is reminiscent of the kink at Ile^{17} found in the Vpu transmembrane helix and identified as a structural determinant of Vpu ion channel activity (68, 69). The presence of the pore-lining residue 17 (28) in this p7 turn indicates that it constitutes an essential structural determinant for p7 ion channel functioning. This turn probably constitutes a flexible link between the rigid N-terminal and TM1 helices that can be considered as the two distinct components of a single transmembrane helix kinked by the 15–18 turn. This conserved flexibility in any genotype suggests the existence of some rigid body movements of α-helices, which are expected to occur upon p7 assembly and/or p7 pore opening and closing.

Another interesting finding is the larger length of the cytosolic loop bearing the essential dibasic motif. Such a loop could allow TM1 and TM2 to reorient relative to each other, which might be triggered by p7 oligomerization and/or ion channel function, as has been proposed above. The conserved bending of the TM2 helix could also play an essential role in these structural changes. Furthermore, TM2 is likely to be involved in the interaction of p7 with other viral or cell factors. This interaction is also expected for the highly conserved unstructured p7 C terminus, which, in all likelihood, is accessible at the membrane surface.

The physicochemical properties of the N-terminal helix appear to be well conserved in any genotype. Its role is presently unclear, but, by analogy with Vpu cytoplasmic helices, it could be involved in the regulation of the lifetime of the p7 channel in its conductive state (70) and/or cation selectivity.

The p7 ion channel has been reported to be activated by low pH (71), and, by analogy to the pH-dependent M2 proton channel of influenza virus, His^{17} has been suggested to play the role of pH sensor (26, 71). However, in contrast to the M2 channel, which only permits proton conductance, p7 is permeable to sodium and potassium (19) (this study). It was reported recently that p7 from genotypes 3–5 encodes a H*XXX*(Y/W) motif (position 17–21) (72). This motif is reminiscent of the H*XXX*W motif found in the influenza M2 ion channel, where the opening is induced by the protonation of the His^{27} imidazole ring at low pH, which in turn promotes an electrostatic interaction that results in the rotation of the indole ring of Trp^{41} (73). Investigation of the putative role of His^{17} in p7 by reverse genetics, however, only showed slight effect on JFH1 infectivity (72). Although these data suggest that the presence of a histidine or an alternative amino acid like glutamic acid, which is protonated at low pH, is important for the optimal function of p7, such pH sensor residues do not appear to be essential for HCV replication. In addition, His^{17} is not conserved among HCV genotypes because Asn, Gln, or Ala is frequently observed at this position (see Fig. 6*A*). Moreover, the mutation of His^{17} to Ala in the context of synthetic p7 of strain H77 reconstituted into planar lipid bilayer was shown to exhibit wild-type channel activity (28). The presence of a histidine residue at position 17 is, therefore, not required for ion channel activity, but the presence of a polar or neutral residue at this position appears to be mandatory.

Interestingly enough, a histidine residue is observed at position 31 of p7 in various genotypes (Fig. 6*A*), whereas the most frequently observed residue at this position protruding into the putative ion channel lumen is a tyrosine. One might wonder whether this histidine residue, when present, could play a pH sensor role in the opening of the p7 channel. In fact, the mutation of His^{31} to Tyr in the context of JFH1 moderately increased assembly, release, and infectivity of JFH1 virus particles (14). Moreover, the reverse mutation, Y31H, in the context of the Jc1 chimera (*i.e.* including p7 of the J6 strain) did not significantly affect infectious particle production. Finally, the non-natural mutations H31F and H31L did not significantly affect virus particle production (7). Although these data imply that the side chain of amino acid 31 modulates the efficiency of p7-dependent virus production, they do not support a role of a pH sensor for this residue. It should be noted that the p7 sequences of several genotypes (2a, 2b, 2c, 6a, 6d, and 6h; Fig. 6*A*) do not include any histidine or other charged residue in the first p7 transmembane helix. Put together, these data indicate that the opening of the p7 pore is likely to be pH-independent.

Intriguingly, it appears that none of the putative pore-lining residues studied to date by mutagenesis seems to be really essential for p7 ion channeling *in vitro*. Little attention has been paid, however, to residues 24 and 25. As has been mentioned previously, positions 24 and/or 25, expected to protrude into the p7 pore, are clearly hydrophobic in any genotype. In the oligomeric structure of p7, the side chain of these residues should form a ring of hydrophobic side chains. Similarly, position 27, predominantly occupied by a cysteine residue (see "Results"), and position 28, occupied by hydrophobic residues in any genotype, are also expected to form a ring of hydrophobic side chains within the p7 pore lumen. These adjacent hydrophobic rings within the center of the membrane channel obviously form an energetic barrier to ion permeation, which must be overcome to allow ions to translocate. The presence of a hydrophobic ring is reminiscent of that observed in various ion channels like the nicotinic acetylcholine receptor (74), the bacterial K^+ channel (75), and the MscL ion channel (76). In these channels, the removal of the hydrophobic barrier to ion permeation arises from the rigid body movements of α-helical segments, triggering the opening of the channel.

It is, therefore, tempting to draw a parallel for the gating of p7, which might obey a similar mechanism. Unfortunately,

except for the C27A mutation studied here and yielding wild-type activity, virtually no mutation at these positions has been reported hitherto. It is worth noting that, whereas the F25A point mutation had no detectable effect, the recombinant triple mutant F22A/F25A/F26A of p7 from strain J4 was recently reported to exhibit a surprising increase of channel activity in a liposome assay (26). Because this triple mutation did not affect the ability of p7 to form oligomeric structures, it is tempting to propose that the reduction of hydrophobicity of residues around position 24 decreases the overall strength of the putative hydrophobic ring, hence facilitating the opening of the p7 channel.

According to this gating mechanism, one can expect that a decrease of the hydrophobicity at positions 24 and/or 25, as well as 27 and/or 28, should increase the p7 ion channel activity. On the other hand, one can speculate that the fully conserved amino acids Trp^{30} and Tyr^{42}, which were demonstrated to be key residues involved in the function of p7 (7), might play a major role in the movement of the helical segments that would be required for the opening of p7 channel. One can imagine that the aromatic ring stacking between Trp^{30} and Tyr^{42}, which contributes to the overall stability of the helix TM1-TM2 bundle in the p7 monomer, could be released and might participate in intermolecular interactions. Similar changes from intra- to intermolecular interaction could also be hypothesized for the side chains of the fully conserved Trp^{48} and Leu^{52}, with the possible participation of other genotype-dependent residues (see "Results"). Concomitant movements of α-helical segments thus might occur, leading to major changes in the structural organization of the p7 channel, and related to the pore opening and closing.

In summary, the structural and functional studies reported here provide the first detailed structural analysis of the p7 monomer. The structural features of the N-terminal and TM1 helices that can be considered as the two distinct components of a single transmembrane helix kinked by the 15–18 turn are likely to be determinants of the ion channel activity. This turn, which includes pore-lining residue 17, is likely to be related to the gating of the ion channel. The absence of an obvious conservation of specific hydrophilic residues lining the lumen of the p7 pore at positions 17, 21, 27, and 31 contrasts with the fully conserved hydrophobic nature of residues at position 24/25, which should form a hydrophobic ring acting as an energetic barrier to ion permeation, possibly together with position 27/28. These features, together with the full conservation of several specific residues involved in essential p7 structural elements, suggest that important movements of structured segments might be required for p7 channel opening and closing. The p7 monomer model reported here provides an experimental template for further investigations of ion channel gating mechanism in p7 oligomers, notably by means of MD simulations in phospholipid bilayer. Finally, the substantial intra- and intergenotype variability of pore-lining hydrophilic amino acids means that anti-HCV drugs targeting these residues would rapidly induce viral resistance. The development of new drugs, therefore, should focus on compounds targeting strictly conserved residues involved in structural elements essential for p7 oligomerization and function and/or interactions of p7 TM-helices, p7 monomers, or other viral or cellular proteins.

Acknowledgments—We gratefully acknowledge Claire Noirot and Annie Chaboud for technical assistance in molecular biology, Eva Pebay-Peyroula and Dominique Cannella for crystallization assays, Rob Ruigrok and Guy Schoehn for microscopy assays, Michel Becchi for the mass spectroscopy measurements, Christophe Combet for bioinformatics support, and the Analytical UltraCentrifugation platform of the Partnership for Structural Biology Grenoble. CD experiments were performed on the platform "Production et Analyse de Protéines" of the IFR 128 BioSciences Gerland-Lyon Sud. The NMR facility used in this study was funded by the Région Rhône-Alpes (France), CNRS, and the Universities of Lyon and Grenoble. We thank the group of Beat Meier (ETH Zurich) for recording the solid-state NMR spectra.

REFERENCES

1. Poynard, T., Yuen, M. F., Ratziu, V., and Lai, C. L. (2003) *Lancet* **362,** 2095–2100
2. Simmonds, P., Bukh, J., Combet, C., Deléage, G., Enomoto, N., Feinstone, S., Halfon, P., Inchauspé, G., Kuiken, C., Maertens, G., Mizokami, M., Murphy, D. G., Okamoto, H., Pawlotsky, J. M., Penin, F., Sablon, E., Shin-I, T., Stuyver, L. J., Thiel, H. J., Viazov, S., Weiner, A. J., and Widell, A. (2005) *Hepatology* **42,** 962–973
3. Combet, C., Garnier, N., Charavay, C., Grando, D., Crisan, D., Lopez, J., Dehne-Garcia, A., Geourjon, C., Bettler, E., Hulo, C., Le Mercier, P., Bartenschlager, R., Diepolder, H., Moradpour, D., Pawlotsky, J. M., Rice, C. M., Trépo, C., Penin, F., and Deléage, G. (2007) *Nucleic Acids Res.* **35,** D363–D366
4. Lindenbach, B. D., Thiel, H. J., and Rice, C. M. (2007) in *Fields Virology*, 5th Ed., Vol. 1 (Knipe, D. M., and Howley, P. M., eds) pp. 1101–1152, Lippincott-Raven Publishers, Philadelphia, PA
5. Moradpour, D., Penin, F., and Rice, C. M. (2007) *Nat. Rev. Microbiol.* **5,** 453–463
6. Carrère-Kremer, S., Montpellier, C., Lorenzo, L., Brulin, B., Cocquerel, L., Belouzard, S., Penin, F., and Dubuisson, J. (2004) *J. Biol. Chem.* **279,** 41384–41392
7. Steinmann, E., Penin, F., Kallis, S., Patel, A. H., Bartenschlager, R., and Pietschmann, T. (2007) *PLoS Pathog.* **3,** e103
8. Carrère-Kremer, S., Montpellier-Pala, C., Cocquerel, L., Wychowski, C., Penin, F., and Dubuisson, J. (2002) *J. Virol.* **76,** 3720–3730
9. Isherwood, B. J., and Patel, A. H. (2005) *J. Gen. Virol.* **86,** 667–676
10. Jones, C. T., Murray, C. L., Eastman, D. K., Tassello, J., and Rice, C. M. (2007) *J. Virol.* **81,** 8374–8383
11. Sakai, A., Claire, M. S., Faulk, K., Govindarajan, S., Emerson, S. U., Purcell, R. H., and Bukh, J. (2003) *Proc. Natl. Acad. Sci. U.S.A.* **100,** 11646–11651
12. Zhong, J., Gastaminza, P., Cheng, G., Kapadia, S., Kato, T., Burton, D. R., Wieland, S. F., Uprichard, S. L., Wakita, T., and Chisari, F. V. (2005) *Proc. Natl. Acad. Sci. U.S.A.* **102,** 9294–9299
13. Murray, C. L., Jones, C. T., Tassello, J., and Rice, C. M. (2007) *J. Virol.* **81,** 10220–10231
14. Brohm, C., Steinmann, E., Friesland, M., Lorenz, I. C., Patel, A., Penin, F., Bartenschlager, R., and Pietschmann, T. (2009) *J. Virol.* **83,** 11682–11693
15. Griffin, S. D., Harvey, R., Clarke, D. S., Barclay, W. S., Harris, M., and Rowlands, D. J. (2004) *J. Gen. Virol.* **85,** 451–461
16. Cook, G. A., and Opella, S. J. (2010) *Eur. Biophys. J.* **39,** 1097–1104
17. Gonzalez, M. E., and Carrasco, L. (2003) *FEBS Lett.* **552,** 28–34
18. Pavlović, D., Neville, D. C., Argaud, O., Blumberg, B., Dwek, R. A., Fischer, W. B., and Zitzmann, N. (2003) *Proc. Natl. Acad. Sci. U.S.A.* **100,** 6104–6108
19. Premkumar, A., Wilson, L., Ewart, G. D., and Gage, P. W. (2004) *FEBS Lett.* **557,** 99–103
20. Griffin, S. D., Beales, L. P., Clarke, D. S., Worsfold, O., Evans, S. D., Jaeger,

J., Harris, M. P., and Rowlands, D. J. (2003) *FEBS Lett.* **535,** 34–38
21. Steinmann, E., Whitfield, T., Kallis, S., Dwek, R. A., Zitzmann, N., Pietschmann, T., and Bartenschlager, R. (2007) *Hepatology* **46,** 330–338
22. Griffin, S., Stgelais, C., Owsianka, A. M., Patel, A. H., Rowlands, D., and Harris, M. (2008) *Hepatology* **48,** 1779–1790
23. Luik, P., Chew, C., Aittoniemi, J., Chang, J., Wentworth, P., Jr., Dwek, R. A., Biggin, P. C., Vénien-Bryan, C., and Zitzmann, N. (2009) *Proc. Natl. Acad. Sci. U.S.A.* **106,** 12712–12716
24. Clarke, D., Griffin, S., Beales, L., Gelais, C. S., Burgess, S., Harris, M., and Rowlands, D. (2006) *J. Biol. Chem.* **281,** 37057–37068
25. Patargias, G., Zitzmann, N., Dwek, R., and Fischer, W. B. (2006) *J. Med. Chem.* **49,** 648–655
26. StGelais, C., Foster, T. L., Verow, M., Atkins, E., Fishwick, C. W., Rowlands, D., Harris, M., and Griffin, S. (2009) *J. Virol.* **83,** 7970–7981
27. Haqshenas, G., Dong, X., Ewart, G., Bowden, S., and Gowans, E. J. (2007) *Virology* **360,** 17–26
28. Chew, C. F., Vijayan, R., Chang, J., Zitzmann, N., and Biggin, P. C. (2009) *Biophys. J.* **96,** L10–L12
29. Combet, C., Blanchet, C., Geourjon, C., and Deléage, G. (2000) *Trends Biochem. Sci.* **25,** 147–150
30. Thompson, J. D., Higgins, D. G., and Gibson, T. J. (1994) *Nucleic Acids Res.* **22,** 4673–4680
31. Saint, N., Montserret, R., Chipot, C., and Penin, F. (2009) *Methods Mol. Biol.* **510,** 125–143
32. Saint, N., Lou, K. L., Widmer, C., Luckey, M., Schirmer, T., and Rosenbusch, J. P. (1996) *J. Biol. Chem.* **271,** 20676–20680
33. Hodgkin, A. L., and Huxley, A. F. (1947) *J. Physiol.* **106,** 341–367
34. Le Dain, A. C., Saint, N., Kloda, A., Ghazi, A., and Martinac, B. (1998) *J. Biol. Chem.* **273,** 12116–12119
35. Hamill, O. P., Marty, A., Neher, E., Sakmann, B., and Sigworth, F. J. (1981) *Pflugers Arch.* **391,** 85–100
36. Salvay, A. G., and Ebel, C. (2006) in *Analytical Ultracentrifugation VIII* (Wondrey, C., and Cölfen, H., eds) *Progr. Colloid Polymer Sci.* Vol. 131, pp. 399–419, Springer, New York
37. Whitmore, L., and Wallace, B. A. (2004) *Nucleic Acids Res.* **32,** W668–W673
38. Penin, F., Geourjon, C., Montserret, R., Böckmann, A., Lesage, A., Yang, Y. S., Bonod-Bidaud, C., Cortay, J. C., Nègre, D., Cozzone, A. J., and Deléage, G. (1997) *J. Mol. Biol.* **270,** 496–510
39. Favier, A., Brutscher, B., Blackledge, M., Galinier, A., Deutscher, J., Penin, F., and Marion, D. (2002) *J. Mol. Biol.* **317,** 131–144
40. Melckebeke, H. V., Vreuls, C., Gans, P., Filée, P., Llabres, G., Joris, B., and Simorre, J. P. (2003) *J. Mol. Biol.* **333,** 711–720
41. Wuthrich, K. (1986) *NMR of Proteins and Nucleic Acids,* John Wiley & Sons, Inc., New York
42. Medvedeva, S., Simorre, J. P., Brutscher, B., Guerlesquin, F., and Marion, D. (1993) *FEBS Lett.* **333,** 251–256
43. Merutka, G., Dyson, H. J., and Wright, P. E. (1995) *J. Biomol. NMR* **5,** 14–24
44. Thanabal, V., Omecinsky, D. O., Reily, M. D., and Cody, W. L. (1994) *J. Biomol. NMR* **4,** 47–59
45. Schwieters, C. D., Kuszewski, J. J., Tjandra, N., and Clore, G. M. (2003) *J. Magn. Reson.* **160,** 65–73
46. Koradi, R., Billeter, M., and Wüthrich, K. (1996) *J. Mol. Graph.* **14,** 51–55
47. Laskowski, R. A., Rullmannn, J. A., MacArthur, M. W., Kaptein, R., and Thornton, J. M. (1996) *J. Biomol. NMR* **8,** 477–486
48. Vakser, I. A., Matar, O. G., and Lam, C. F. (1999) *Proc. Natl. Acad. Sci. U.S.A.* **96,** 8477–8482
49. Humphrey, W., Dalke, A., and Schulten, K. (1996) *J. Mol. Graph.* **14,** 33–38
50. Phillips, J. C., Braun, R., Wang, W., Gumbart, J., Tajkhorshid, E., Villa, E., Chipot, C., Skeel, R. D., Kalé, L., and Schulten, K. (2005) *J Comput. Chem.* **26,** 1781–1802
51. MacKerell, A. D., Bashford, D., Bellott, M., Jr., Dunbrack, R. L., Evanseck, J. D., Field, M. J., Fischer, S., Gao, J., Guo, H., Ha, S., Joseph-McCarthy, D., Kuchnir, L., Kuczera, K., Lau, F. T. K., Mattos, C., Michnick, S., Ngo, T., Nguyen, D. T., Prodhom, B., Reiher, W. E., Roux, B., Schlenkrich, M., Smith, J. C., Stote, R., Straub, J., Watanabe, M., Wiorkiewicz-Kuczera, J., Yin, D., and Karplus, M. (1998) *J. Phys. Chem. B* **102,** 3586–3616
52. Feller, S. E., Zhang, Y. H., Pastor, R. W., and Brooks, B. R. (1995) *J. Chem. Phys.* **103,** 4613–4621
53. Darden, T. A., York, D. M., and Pedersen, L. G. (1993) *J. Chem. Phys.* **98,** 10089–10092
54. Tuckerman, M. E., Berne, B. J., and Martyna, G. J. (1992) *J. Phys. Chem.* **97,** 1990–2001
55. Møller, J. V., and le Maire, M. (1993) *J. Biol. Chem.* **268,** 18659–18672
56. Buck, M. (1998) *Q. Rev. Biophys.* **31,** 297–355
57. Montserret, R., Aubert-Foucher, E., McLeish, M. J., Hill, J. M., Ficheux, D., Jaquinod, M., van der Rest, M., Deléage, G., and Penin, F. (1999) *Biochemistry* **38,** 6479–6488
58. Wishart, D. S., Sykes, B. D., and Richards, F. M. (1992) *Biochemistry* **31,** 1647–1651
59. Frishman, D., and Argos, P. (1995) *Proteins* **23,** 566–579
60. Chipot, C., Jaffe, R., Maigret, B., Pearlman, D. A., and Kollman, P. A. (1996) *J. Am. Chem. Soc.* **118,** 11217–11224
61. Castelain, S., Bonte, D., Penin, F., François, C., Capron, D., Dedeurwaerder, S., Zawadzki, P., Morel, V., Wychowski, C., and Duverlie, G. (2007) *J. Med. Virol.* **79,** 144–154
62. Cordes, F. S., Tustian, A. D., Sansom, M. S., Watts, A., and Fischer, W. B. (2002) *Biochemistry* **41,** 7359–7365
63. Helluin, O., Dugast, J. Y., Molle, G., Mackie, A. R., Ladha, S., and Duclohier, H. (1997) *Biochim. Biophys. Acta* **1330,** 284–292
64. Saint, N., Marri, L., Marchini, D., and Molle, G. (2003) *Peptides* **24,** 1779–1784
65. Grice, A. L., Kerr, I. D., and Sansom, M. S. (1997) *FEBS Lett.* **405,** 299–304
66. Fischer, W. B., Forrest, L. R., Smith, G. R., and Sansom, M. S. (2000) *Biopolymers* **53,** 529–538
67. Chew, C. F., Guy, A., and Biggin, P. C. (2008) *Biophys. J.* **95,** 5627–5636
68. Park, S. H., Mrse, A. A., Nevzorov, A. A., Mesleh, M. F., Oblatt-Montal, M., Montal, M., and Opella, S. J. (2003) *J. Mol. Biol.* **333,** 409–424
69. Park, S. H., De Angelis, A. A., Nevzorov, A. A., Wu, C. H., and Opella, S. J. (2006) *Biophys. J.* **91,** 3032–3042
70. Montal, M. (2003) *FEBS Lett.* **552,** 47–53
71. StGelais, C., Tuthill, T. J., Clarke, D. S., Rowlands, D. J., Harris, M., and Griffin, S. (2007) *Antiviral Res.* **76,** 48–58
72. Meshkat, Z., Audsley, M., Beyer, C., Gowans, E. J., and Haqshenas, G. (2009) *J. Viral Hepat.* **16,** 187–194
73. Tang, Y., Zaitseva, F., Lamb, R. A., and Pinto, L. H. (2002) *J. Biol. Chem.* **277,** 39880–39886
74. Unwin, N. (1995) *Nature* **373,** 37–43
75. Perozo, E., Cortes, D. M., and Cuello, L. G. (1999) *Science* **285,** 73–78
76. Biggin, P. C., and Sansom, M. S. (2001) *Curr. Biol.* **11,** R364–R366
77. Kuiken, C., Mizokami, M., Deleage, G., Yusim, K., Penin, F., Shin-I, T., Charavay, C., Tao, N., Crisan, D., Grando, D., Dalwani, A., Geourjon, C., Agrawal, A., and Combet, C. (2006) *Hepatology* **43,** 1157–1165

NMR Structure and Ion Channel Activity of the p7 Protein from Hepatitis C Virus

Roland Montserret, Nathalie Saint, Christophe Vanbelle, Andrés Gerardo Salvay, Jean-Pierre Simorre, Christine Ebel, Nicolas Sapay, Jean-Guillaume Renisio, Anja Böckmann, Eike Steinmann, Thomas Pietschmann, Jean Dubuisson, Christophe Chipot and François Penin

J. Biol. Chem. 2010. 285:31446-31461.
doi: 10.1074/jbc.M110.122895 originally published online July 28, 2010
